Gerald Gerlach | Wolfram Dötzel

Introduction to Microsystem Technology

A Guide for Students

Solutions for exercises

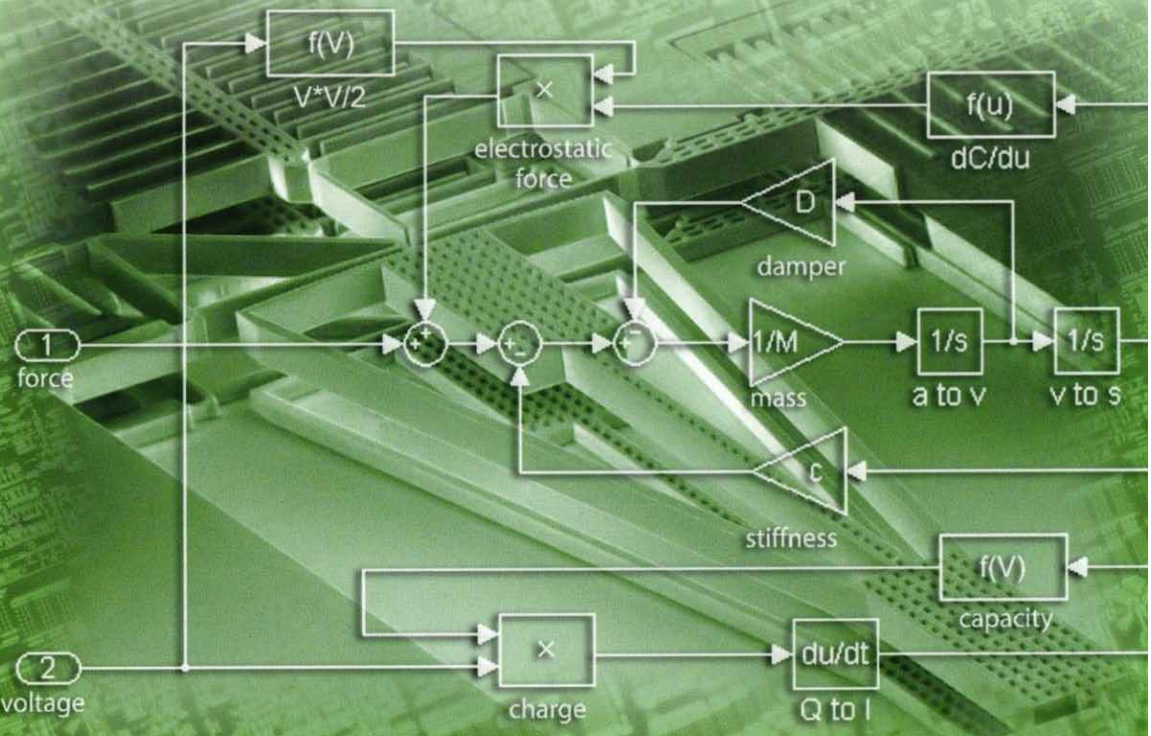

Companion Website

WILEY

The Wiley Microsystem and Nanotechnology Series | Ronald Pethig, Series Editor

Solutions to the exercises of chapter 1: Introduction

Exercise 1.1

Function principles of microsystems are shown in Figure 1.2 in the book:

a) The silicon strain gauge changes its resistance R_0 in relation to strain ε (see Section 7.2.5a in the book):
   Strain ε → resistance $R = R_0 + \Delta R(\varepsilon)$.

b) Between the two sides of the thinned pressure plate of the silicon sensor chip acts differential pressure p. This leads to a deformation, i.e. a displacement of the pressure plate. On the surface - in the different areas of the pressure plate – the bending causes tensile stress ($\sigma > 0$) or compressive stress ($\sigma < 0$), or strained ($\varepsilon > 0$) or compressed ($\varepsilon < 0$) areas, respectively. The resistors that are diffused into the pressure sensor chip will change according to Example 1.1a in the book. Typically, a WHEATSTONE measuring bridge is used to transform the change in resistance into an electrical output voltage (see Example 7.8 in the book). Thus, the function principle corresponds to that in Figure 7.21 from the book.

c) The measuring acceleration displaces the cantilever attached to the substrate at one side of the gate due to the cantilever`s inertia. A change in the distance between the cantilever located on the gate potential and the source-drain area causes a change in the electric field strength and, consequently, in the current between source and drain. This corresponds to the operational principle of a field effect transistor with changeable gate voltage.
   Acceleration → Displacement of cantilever → Changed current between source and drain.

d) The working principle of this pressure sensor corresponds to that in Figure 1.2b in the book. However, in this case the pressure plate is not produced by local thinning, but by the silicon wafer itself, which is fixed to a polycrystalline silicon ring (in 1970, Si wafers still had a diameter of about ½ …¾ inch).

Exercise 1.2

a) Piezoresistive pressure sensor in Figure 7.23a in the book:
   Function elements: - Bending plate
   - Thick mounting rim
   - Piezoresistors
   Components: - Piezoresistive pressure sensor

b) Micro-pump according to Figure 6.13b in the book:
   Function elements: - Inlet channel (R_E, L_E)
   - Outlet channel (R_A, L_A)
   - Inlet valve (R_{V1}, C_{V1})
   - Outlet valve (R_{V2}, C_{V2})
   - Pressure source (Δp_S, C_{11})
   Components: - Micro pumps

c) Bolometer array (Figures 10.2 and 10.3 in the book):
   Function elements: - Resistor (bolometer) element
   - Absorption layer
   - Contact columns
   - Radiation reflector
   - Contacting
   Components: - CMOS evaluation circuit
   - Infrared bolometer

Exercise 1.3

See in the Internet.

Solutions to the exercises of chapter 2: Scaling and Similarity

Exercise 2.1

Efficiency η is a unitless number that describes the ratio between output and input energy of a system:

$$\eta = W_{\text{out}} / W_{\text{in}} .$$

For an electro-mechanical drive, it would be

$$\eta = W_{\text{mech}} / W_{\text{el}} .$$

Exercise 2.2

The REYNOLDS number describes the ratio between the force of inertia acting on fluidic particles in a flowing fluid and the viscous friction force.

As a model, we use the fluid volume in a fluidic channel where a square plate with area $A = a \cdot a$ is moved on its upper side at speed u. The distance between the moveable plate and the fixed lower side of the fluidic channel ($u = 0$) is assumed to be a, too. A linear velocity profile will be formed between the moved plate and the fixed lower side of the fluidic channel (see Figure 6.6a in the book). Friction force F_{R} for the plate's movement is

$$F_{\text{R}} = \tau \cdot A = \mu \cdot \frac{u}{a} \cdot A = \mu \cdot \frac{u}{a} \cdot a^2 = \mu \cdot u \cdot a .$$

Here, τ is the shear stress in the fluid and μ its dynamic viscosity.

Force of inertia F_{m} can be calculated using the kinetic energy. In order to accelerate the fluid volume under the moved plate by speed u, the following energy has to be supplied

$$E_{\text{kin}} = \frac{1}{2} \cdot m \cdot u^2 = F_{\text{m}} \cdot s .$$

Here, $m = \rho \cdot V = \rho \cdot a^3$ and s is the average distance covered by the fluid volume under the plate. If the plate moves by distance a, this means that $s = a/2$. It results that

$$F_{\text{m}} = \frac{E_{\text{kin}}}{s} = \frac{1}{2} \cdot m \cdot u^2 \cdot \frac{2}{a} = \frac{m \cdot u^2}{a} = \frac{\rho \cdot a^3 \cdot u^2}{a} = \rho \cdot a^2 \cdot u^2 .$$

The resulting REYNOLDS number thus becomes

$$Re = \frac{F_{\text{m}}}{F_{\text{R}}} = \frac{\rho \cdot a^2 \cdot u^2}{\mu \cdot u \cdot a} = \frac{\rho}{\mu} \cdot a \cdot u = \frac{a \cdot u}{\nu} .$$

Here, $\nu = \mu/\rho$ is the kinetic viscosity of the fluid.

Exercise 2.3

A dust particle adheres to the ceiling if its weight F_G has a lower value than the electrostatic attractive force F_{el} to the ceiling:

$$|F_{\text{G}}| < |F_{\text{el}}| \tag{1}$$

The weight amounts to

$$F_{\text{G}} = m \cdot g = \rho \cdot \ell^3 g \tag{2}$$

where ρ is the specific density, ℓ the edge length of the dust particle and g the earth acceleration ($g = 9.81\ \text{ms}^{-2}$).

The electrostatic force results from equations 2.3 and 2.4 from the book and becomes

$$F_{\text{el}} = -\frac{\text{d}W_{\text{el}}}{\text{d}x} \tag{3}$$

with

$$W_{\text{el}} = \frac{1}{2} \frac{Q^2}{C} ,$$

where Q is the charge of the dustcorn surface, C the capacitance, and x the distance between dust particle and ceiling. Surface charge Q on one side of the dust particle is given by the number of the surface atoms $n = (\ell / a)^2$:

$$Q = 2 \cdot \left(\frac{\ell}{a} \right)^2 \cdot e$$

Factor 2 includes the fact, that the silicon lattice is formed by two cubic face-centred base lattices (see Table 3.4 in the book). Capacitance C corresponds to

$$C = \varepsilon_0 \cdot \frac{\ell^2}{x}. \tag{4}$$

Applying equations 3 to 4, it results that

$$F_{\text{el}} = -\frac{\mathrm{d}W_{\text{el}}}{\mathrm{d}x} = -\frac{\mathrm{d}}{\mathrm{d}x}\left(\frac{Q^2}{2C} \right) = -\frac{\mathrm{d}}{\mathrm{d}x}\left(\frac{2e^2 \cdot \ell^2}{\varepsilon_0 a^4} x \right) = -\frac{2e^2 \ell^2}{\varepsilon_0 a^4}. \tag{5}$$

For the conditions in equation 1 and applying equations 2 and 5, it results that:

$$\rho \cdot \ell^3 \cdot g < \frac{2e^2 \ell^2}{\varepsilon_0 a^4} \qquad \text{or} \qquad \ell < \frac{2e^2}{\rho \cdot g \cdot \varepsilon_0 a^4} \sim \frac{1}{a^4}. \tag{6}$$

Equation (6) shows that - in the case that the dust particle adheres to the ceiling - the admissible dimension scales with a^{-4}. Using the values of e and ε_0 in Appendix A1 in the book, $\rho_{\text{Si}} = 2\,300\ \text{kgm}^{-3}$ and $a = 0.543$ nm, this specific case results in:

$$\ell = \frac{2 \cdot \left(1.6022 \cdot 10^{-19}\right)^2 \cdot (\text{As})^2}{2.300\,\text{kgm}^{-3} \cdot 9.81\,\text{ms}^{-2} \cdot 8.8542 \cdot 10^{-12}\,\text{As}(\text{Vm})^{-1} \cdot \left(0.543 \cdot 10^{-9}\right)^4 \text{m}^4} \tag{7}$$

and with 1 Ws = 1 $\text{kgm}^2\text{s}^{-2}$

$$\ell < 3.03 \cdot 10^6\,\text{m}.$$

At first sight, this result appears to be wrong as the idea of a cube with an edge length of about 3 000 km that sticks to a ceiling only by electrostatic forces is hard to grasp. In our case, however, not the result is wrong, but the assumption that the cube only has a distance of $a = 0.543$ nm to the ceiling! If we look at a more realistic distance of $a^* = 1$ µm and use the scaling factor $\lambda_a = a^*/a = 1.842$ and the ratio

$$\ell \cdot a^4 = \ell^* \cdot a^{*4} = \frac{2e}{\rho \cdot g \cdot \varepsilon_0}$$

an admissible dust particle size will result:

$$\ell^* < \ell \cdot \left(\frac{a}{a^*} \right)^4 = \ell \cdot \frac{1}{\lambda_a^4} = 3.03 \cdot 10^6\,\text{m} \cdot \left(\frac{0.543\,\text{nm}}{1.000\,\text{nm}} \right)^4 = 0.264\,\mu\text{m}.$$

This result much better corresponds to our own experience of that only small particles can adhere to the ceiling. The average distance of 1 µm between dust particle and ceiling is given by the surface roughness. The following remark is important regarding the result in equation 7. If we succeed in establishing an atomically close contact between two bodies with large areas, it is possible to generate very large electrostatic attraction. Wafer preparation for anodic bonding and for silicon direct bonding (see Sections 4.8.2-3 in the book) makes use of this fact.

Exercise 2.4

Resonance angular frequency ω_0 of the oscillating spring-mass-system in Figure 2.4 in the book is

$$\omega_0 = \frac{1}{\sqrt{mn}}.$$

With

$$m = \rho \cdot V_m = \rho \cdot a^3$$

for a cubic mass (ρ density, V_m volume of the mass, a edge dimension of the mass cube), and

$$n = \frac{\ell}{EA} = \frac{\ell}{E \cdot b^2}$$

for a spring with a square cross-section (ℓ spring length, E Young's modulus, A spring cross-sectional area, b edge length of the spring cross-section), it results that

$$\omega_0 = \sqrt{\frac{E \cdot b^2}{\rho \cdot a^3 \cdot \ell}}.$$

Using the reduction coefficients λ_a, λ_b und λ_ℓ for the geometric dimensions a, b and ℓ

$$\lambda_a = a_m/a_0, \quad \lambda_b = b_m/b_0, \quad \lambda_\ell = \ell_m/\ell_0$$

(indices 0 and m characterize the original and the miniaturized arrangement), it results that

$$\frac{\omega_{0m}}{\omega_{00}} = \frac{\lambda_b}{\sqrt{\lambda_a^3 \cdot \lambda_\ell}}.$$

A larger dynamic range requires

$$\frac{\omega_{0m}}{\omega_{00}} > 1.$$

For miniaturization $(\lambda_a, \lambda_b, \lambda_\ell < 1)$, this can only be achieved by using λ_a und λ_ℓ. This means that for a larger dynamic range, mass m and spring length ℓ should be reduced.

Solutions to the exercises of chapter 3: Materials

Exercise 3.1

Using equation 3.5 from the book, the right angle α = 90° between the two areas (h_1, k_1, ℓ_1) and (h_2, k_2, ℓ_2) requires the condition

$$\alpha = 90° = \arccos 0$$

or

$$h_1 h_2 + k_1 k_2 + \ell_1 \ell_2 = 0\,. \tag{8}$$

{100} silicon:

As only one of the parameters h_1, k_1 or ℓ_1 adopts the value zero for {100} planes and as the corresponding value h_2, k_2 or ℓ_2 for {111} planes is ± 1, it is not possible to fulfil the condition in equation 8. The occurring angles can only be

$$\alpha = \arccos\frac{\pm 1}{\sqrt{3}} = 54.74° \text{ or } 125.26°\,.$$

{110} silicon:

If it is possible to find combinations for $\ell_1 = 0$ where $h_1 h_2 = -k_1 k_2$, for instance, we can meet the requirement of equation 8.

Examples:

(110) or $(\bar{1}\bar{1}0)$ and $(\bar{1}11)$ or $(1\bar{1}1)$ or $(\bar{1}1\bar{1})$ or $(1\bar{1}\bar{1})$

$(\bar{1}10)$ or $(1\bar{1}0)$ and (111) or $(\bar{1}\bar{1}1)$ or $(11\bar{1})$ or $(\bar{1}\bar{1}\bar{1})$

{111} silicon:

As it applies to any two {111} planes that

$$|h_1 h_2| = |k_1 k_2| = |\ell_1 \ell_2| = 1\,,$$

the condition in equation 8 cannot be fulfilled.

Exercise 3.2

According to Section 4.6 in the book, etchings in silicon that start from the wafer surface only have boundary planes with an inclination angle of maximum 90°. Undercuttings, i.e. structures that become wider with depth, cannot be produced without specific additional processes. In a (001) silicon wafer, only four {111} planes cut across the wafer surface: (111), $(1\bar{1}\bar{1})$, $(11\bar{1})$ and $(\bar{1}\bar{1}1)$.

For (111) wafers, only $(\bar{1}11)$-, $(1\bar{1}1)$and $(11\bar{1})$ planes as well as the (111) bottom plane are potential {111} lateral planes.

For (110) silicon, there are six lateral boundary planes in addition to the (110) bottom plane.

$(\bar{1}11), (1\bar{1}1), (\bar{1}1\bar{1}), (1\bar{1}\bar{1})$: 90.00° for (110) plane

$(111), (\bar{1}\bar{1}\bar{1})$: 35.26° for (110) plane

The planes $(1\bar{1}1)$ and $(\bar{1}1\bar{1})$ are situated at an angle of 70.53° or 109.47°, respectively, in relation to the planes $(\bar{1}11)$ and $(1\bar{1}\bar{1})$. This results in the geometry in Figure 4.33 in the book.

Exercise 3.3

According to equation 3.13 from the book, it applies that

$$\frac{1}{E_{\langle 111\rangle}} = s_{11} - s\frac{h^2k^2 + k^2\ell^2 + h^2\ell^2}{\left(h^2 + k^2 + \ell^2\right)^2}$$

with $h = k = \ell = 1$, $s = 7.08 \cdot 10^{-12}\,\mathrm{m}^2 N^{-1}$ and $s_{11} = 7.68 \cdot 10^{-12}\,\mathrm{m}^2 N^{-1}$. It follows that

$$\frac{1}{E_{\langle 111\rangle}} = 7.68\cdot 10^{-12}\,\mathrm{m^2N^{-1}} - 7.08\cdot 10^{-12}\,\mathrm{m^2N^{-1}}/3 = 5.32\cdot 10^{-12}\,\mathrm{m^2N^{-1}}$$

$$E_{\langle 111\rangle} = 1.88\cdot 10^{11}\,\mathrm{Nm^{-2}}.$$

Exercise 3.4

Using equation 3.16 from the book, the failure probability can be calculated as

$$F(\sigma) = 1 - \exp\left\{-(\sigma/b)^k\right\}.$$

At ambient temperature and according to Table 3.8 from the book, it is valid for {100}-Si that $b = 3.73 \cdot 10^9$ GPa and $k = 6.18$. This results in failure probabilities $F(\sigma)$ for the given tensile stresses:

σ in 10^9 GPa	***F*(σ)**
0.058	$6.7 \cdot 10^{-12}$
0.58	$1.0 \cdot 10^{-5}$
5.8	0.9999998

Exercise 3.5

We can start again from equation 3.25 for the glass body in Figure 3.12 in the book:

$$\underline{v} = (r + sn)\underline{F}\,. \tag{9}$$

We have a deformation step load:

$$u(t) = \begin{cases} 0 & \text{für t} < 0 \\ u_0 & \text{für t} \geq 0 \end{cases} \tag{10}$$

Using complex frequencies *s*, the LAPLACE transformation results in

$$\underline{u}(s) = u_0 \cdot \frac{1}{s}\,. \tag{11}$$

We are looking for the progress of the mechanical stress

$$\sigma(t) = F(t)/A\,. \tag{12}$$

Using equations (9) to (12), it follows that:

$$\underline{\sigma}(s) = \frac{\underline{F}(s)}{A} = \frac{1}{A}\cdot\frac{1}{r+sn} = \underline{v}(s).$$

Applying $\underline{v}(s) = s\cdot\underline{u}(s)$, it follows that

$$\underline{\sigma}(s) = \frac{u_0}{An}\cdot\frac{1}{s+\frac{r}{n}}\,.$$

The LAPLACE inverse transformation, using the relationship

$$\frac{1}{s+\alpha} \leftrightarrow e^{-\alpha t}$$

results in the solution

$$\sigma(t) = \begin{cases} 0 & \text{for } t < 0 \\ \frac{u_0}{An}\cdot e^{-\frac{t}{\tau}} & \text{for } t \geq 0 \end{cases}$$

with a time constant

$$\tau = \frac{n}{r}\,.$$

Due to the deformation at time $t = 0$ a mechanical stress is generated in the glass body, which relaxes over time due to the viscous properties (Picture 1). After an infinitely long time, the mechanical stress is completely eliminated.

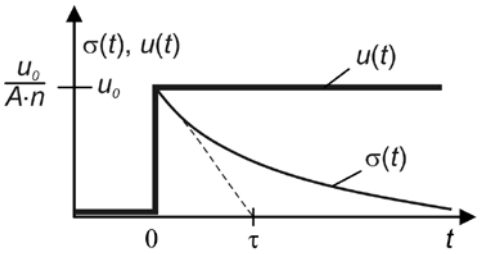

Picture 1: Stress relaxation in glass

Exercise 3.6

We can use equation 3.39 from the book to calculate film stress σ_{PI} in a polyimide layer of a Si wafer:

$$\sigma_{PI} = \frac{1}{6} \frac{E_{Si}}{1-\nu_{Si}} \frac{h_{Si}^2}{h_{PI}} \frac{1}{R}, \tag{13}$$

where E_{Si}, γ_{Si} and h_{Si} are YOUNG's modulus, POISSON's ratio and the thickness of the silicon wafer and h_{PI} is the thickness of the polyimide layer. As the diameter d = 150 mm of the Si wafer is much larger than the bowing of u = 10 µm, it applies for the relationship between the radius of curvature R in equation 13 and the given bowing according to equation 3.39 in the book.

$$\sigma_{PI} = \frac{3}{4} \frac{E_{Si}}{1-\nu_{Si}} \cdot \frac{h_{Si}^2}{h_{PI}} \cdot \frac{u}{d^2}$$

Using the values in Table 3.7 ($E_{Si} = 1.69 \cdot 10^{11}$ N/m²; $\nu_{Si} = 0.063$) and Table 3.10 from the book (h_{Si} = 675 µm), it applies for (100) <110>-oriented silicon that

$$\sigma_{Si} = 9.84 \cdot 10^6 \text{N/m}^2 = 9.84 \text{ MPa}.$$

Solutions to the exercises of chapter 4: Microfabrication

Exercise 4.1

See solution to Exercise 3.2

Exercise 4.2

We start from Figure 4.26 in the book (see picture 2 below) when constructing the etch rate diagram. The sidewalls of the structure, that form together with the wafer surfaces <110>-oriented mask edges, are etched off with an undercutting rate of $R_u = R_{\langle 110 \rangle}$. On both right-hand convex edges, sidewalls will form that are etched off with the maximum undercutting rate of $R_u = R_{max}$.

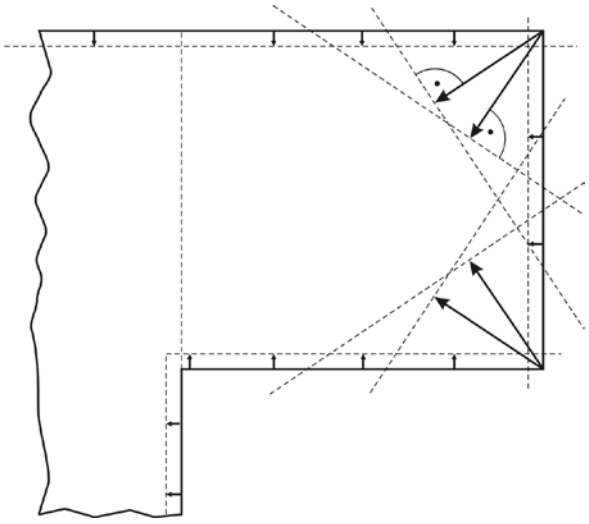

Picture 2: Relevant etch rates R_{max} and $R_{<110>}$

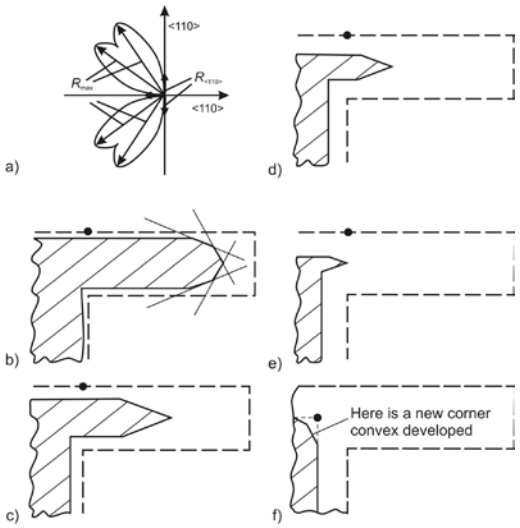

Picture 3: Etching progress for anisotropic etching of the etch mask edges, with compensation mask part a) $t = t_0$; b…f) $t = t_0 \ldots 5t_0$

After time t_0, the undercutting in the different directions amounts to $R_u \cdot t_0$ each (Picture 3a). The structure is formed by the innermost etch fronts (Picture 3b). For the newly formed convex edges, there are no other fast-etching areas, which means that the existing sidewalls will be continuously removed. During the etching process it is possible that certain sidewalls disappear or are incorporated into other sidewalls due to reasons of geometry (Picture 3b→c).

After a certain time, the compensation mask part is completely etched off which means a new convex edge forms (Picture 3e→f). From there, the undercutting process continues analogously.

Exercise 4.3

Picture 4 represents the geometrical relations of pressure plates that are produced using anisotropic wet chemical deep etching or bond-and-etchback.

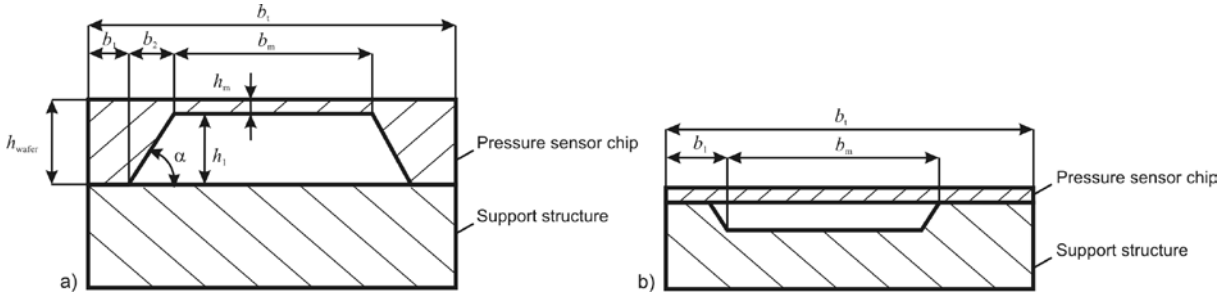

Picture 4: Pressure sensors, produced using a) anisotropic wet chemical deep etching and b) through bonding-and-etchback

Anisotropically etched pressure sensor (Picture 4a):

Total width b_t is

$$b_t = b_m + 2(b_1 + b_2),$$

where b_m is the plate width, b_1 the assembly width, and b_2 the space required for the etching inclination. The latter is related to etching depth h_1 via angle α = 54.74° (see Figure 3.5d in the book):

$$b_2 = h_1/\sqrt{2}\,.$$

The etch depth h_1 results from wafer thickness h_{wafer} and plate thickness h_m and becomes

$$h_1 = h_{wafer} - h_m$$

For a 150 mm-Si-wafer, standard wafer thickness h_{wafer} - according to Table 3.10 from the book – is h_{wafer} = 675 µm.

With the given values h_m = 25 µm, b_m = 500 µm, and b_1 = 100 µm, it results from equations above for the total chip width that

$$b_t = b_m + 2b_1 + 2b_2 = b_m + 2b_1 + \sqrt{2}(h_{wafer} - h_m) = 1.62\,\text{mm}\,.$$

This means that a square sensor chip requires a chip area of $A = b_t^2 = 2.62\ \text{mm}^2$.

Pressure sensor, manufactured through bonding-and-etchback (Picture 4b):

Due to this specific kind of manufacturing, there is no spatial requirement for etching inclinations. Total width b_t thus results in

$$b_t = b_m + 2b_1 = 700\ \mu\text{m}$$

and the required total chip area

$$A = b_t^2 = 0.49\ \text{mm}^2\,.$$

This corresponds to less than 20 % of the chip area that is required for anisotropically etched pressure sensors. In microelectronics, chip prices are almost proportional to chip areas, which mean that there is a correspondingly large cost advantage.

Exercise 4.4

For estimating the projected range R_p, we can assume a symmetric distribution of oxygen ions both after the implantation according to equation 4.51 in the book and the formation of the SIMOX-SiO_2-layer. This means that R_p lies exactly in the middle of the SiO_2-layer:

$$R_p = d_{Si} + \frac{1}{2} d_{SiO_2} = 200\ \text{nm} + 400\ \text{nm}/2 = 400\ \text{nm}\,,$$

where d_{Si} and d_{SiO_2} are the layer thicknesses of the Si- and the SiO_2-layer, respectively. This value corresponds to the interpolated value for the O^+-ion implantation with an energy of 200 KeV in Table 4.17 from the book.

In addition, it follows from equation 4.51 in the book for z = R_p

$$n(R_p) = n_{max} = \frac{n^*}{\sqrt{2\pi}\,\Delta R_p} \quad \text{or} \quad \Delta R_p = \frac{n^*}{\sqrt{2\pi}\cdot n_{max}} \sim \frac{1}{n_{max}}. \tag{14}$$

As no data is provided for n_{max} or any $n(z)$, ΔR_p cannot be calculated based on the given values. Depending on the implantation conditions, the scattering ΔR_p can vary. Typically, R_p mainly depends on energy E and the mass of the implanted ions, and ΔR_p on the ratio of the mass of the implanted ions and the atom lattice. It is quite easy to estimate whether – under the given conditions – real stoichiometric SiO_2 has been formed.

We start from the Si lattice cell in Figure 3.2c in the book, which has 8 corner atoms (that the lattice cell shares with another 7 lattice cells), 6 atoms on side wall (that are shared with the respective adjacent lattice cells) as well as 4 atoms in the volume of the base cell. This means that we have per lattice cell

$$N_{Si} = \frac{1}{8}\cdot 8 + \frac{1}{2}\cdot 6 + 4 = 8$$

Si-atoms. For a complete oxidation, we need two O^+-ions per Si-atom:

$$N_{O^+} = 2\ N_{Si} = 16.$$

This means that the required density of O^+-ions amounts to

$$n_{O^+} = \frac{N_{O^+}}{a^3} = \frac{16}{(0{,}543\ \text{nm})^3} = 1{,}0\cdot 10^{23}\,\text{cm}^{-3},$$

where a is the lattice constant of Si.

According to Figure 4.11 in the book, silicon thickness $d_{Si,implantiert}$ which results in a 400 nm thick SiO_2-layer is

$$d_{Si,implantiert} = 0{,}45\cdot d_{SiO_2} = 180\ \text{nm} = 1.8\cdot 10^5\,\text{cm}^{-1}.$$

Thus, the required implantation dose becomes

$$n^* = n_{O^+}\cdot d_{Si,implantiert} = 1.8\cdot 10^{18}\,\text{cm}^{-2}.$$

This is a good correspondence to the value in the exercise. Deviations are due to the facts that the SiO^2 layer in the SIMOX wafer is amorphous, which means that we cannot assume single-crystalline silicon.

Assuming that for the O^+-implantation during the SIMOX process, the maximum value should correspond to the above concentration of $n_{O^+} = 10^{23}\,\text{cm}^{-3}$, it follows from equation 14 that

$$\Delta R_p = \frac{n^*}{\sqrt{2\pi}\cdot n_{O^+}} = \frac{10^{18}\,\text{cm}^{-2}}{\sqrt{2\pi}\cdot 10^{23}\,\text{cm}^{-3}} = 40\ \text{nm}.$$

This value is half of the value that can be determined according to the reference in Table 4.17 in the book and amounts to 77 nm.

Exercise 4.5

We will look at the arrangement in Figure 4.53 using the geometry variables of Figure E.2 in Appendix E (both see in the book). The adhesion in the case without nubs is determined by the adhesion area $A_B = (\ell - x)\cdot b$. The nubs in Figure 4.53 from the book reduce the adhesion area to

$$A_B = (\ell - x) \cdot b \cdot \lambda_A$$

where λ_A is the scaling factor of the adhesion area ($0 < \lambda_A \leq 1$). Thus, the surface energy in equation E.9 in the book is modified to

$$E_0 = C - \gamma_s (\ell - x) b .$$

A further derivation, analogous to Appendix E, then leads to a modified equation E.12 from the book:

$$E_0 = C - \gamma_s (\ell - x) b$$

Critical length ℓ_{km} of an unsupported cantilever spring according to Figure 4.53b in the book increases in relation to an unstructured arrangement according to

$$\frac{\ell_{km}}{\ell_{k0}} = \sqrt[4]{\frac{1}{\lambda_m}} .$$

For $\lambda_m = 0.01$, for instance, the nub structure will reduce the adhesion area to one hundredth part, and this means that the critical length increases by factor 3.2.

Exercise 4.6

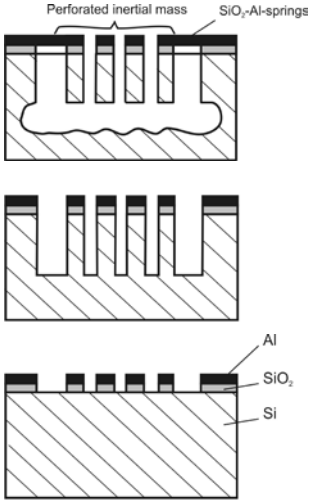

Thermal oxidation
Al vapour deposition
Structuring of the Al- and the SiO_2-layer

DRIE (with passivation of sidewalls)

Isotropic gaseous-phase etching with passivated sidewalls for undercutting/opening-up of bulk structures (on the trench bottom)
Etching of the sidewall passivation. Isotropic gaseous-phase etching of the total structure for undercutting the Al/SiO_2 spring structure

Picture 5: Production of the AIM structure

Exercise 4.7

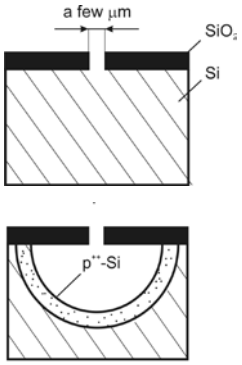

Thermal oxidation
Structuring of the SiO_2-layer

Boron diffusion in Si (B^+-concentration ca. 10^{20} B^+/cm^3) down to a depth of 5 µm

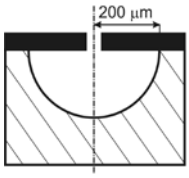

Isotropic Si-etching (wet chemical etching or gaseous-phase etching)

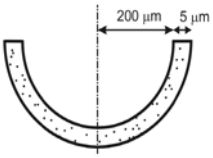

SiO_2 removal
Si-etching with EDP etching solution (selective etch stop on highly-doped p^{++}-Si)

Picture 6: Manufacturing process for hemisphere structure

Exercise 4.7

Processing	Si pressure plate	Poly-Si pressure plate	SiO_2 or Si_3N_4 pressure plate
Two-step processing	BS: Anisotropic wet chemical Si etching (see Figure 4.2 j,k)	FS: Deposition and structuring of a SiO_2 sacrificial layer FS: Deposition of the poly-Si layer BS: Anisotropic wet chemical Si etching to the SiO_2 sacrificial layer BS: SiO_2 sacrificial layer etching	BS: Anisotropic wet chemical Si etching to the SiO_2/Si_3N_4-(etch stop) layer (analogous to Picture 4.2 j,k)
One-sided processing (surface micromachining)	See for instance [KNESE07]: - n-doping of a perforated lattice structure on the surface of a p-Si wafer - Transformation of p-Si underneath the n-Si lattice structure by anodization into porous Si - Creation of a cavern underneath the n-Si lattice by H_2 prebake - Si-Epitaxy layer on self-supporting n-Si lattice	FS: Surface micromachining standard technology according to Figure 4.49 in the book	FS: SiO_2-layer deposition FS: Si_3N_4-layer deposition and structuring (uncovered SiO_2-range in the middle forms sacrificial layer) FS: SiO_2-layer deposition and structuring (etching channel for sacrificial layer etching) FS: Si_3N_4 cover layer (functional layer) FS: SiO_2-sacrificial layer etching via etching channel FS: Anisotropic Si-etching (opening up the V-trench beneath the etched-off SiO_2 sacrificial layer range in order to create space for sufficiently large displacements of the Si_3N_4 pressure plate)
Two-wafer processing (bonding-and-etchback)	Manufacturing as in Picture 4.45		**Wafer #1:** Anisotropic wet chemical etching of Si through SiO_2/Si_3N_4-etch mask **Wafer #2:** SiO_2 or Si_3N_4 deposition **Wafer #1 and #2:** Anodic bonding, etchback of wafer #2 to SiO_2-/Si_3N_4-layer

FS front side, BS back side

[KNESE07] K. Knese, S. Armbruster, H. Benzel, H. Seidel: Neue oberflächenmirkomechanische Technologie zur Herstellung kapazitiver Sensoren auf Basis von porösem Silizium. In: Mikrosystemtechnik Kongress 2007, 15. bis 17. Oktober. Proceedings. Berlin, Offenbach: VDE-Verlag 2007. S. 131 – 134.

Exercise 4.9

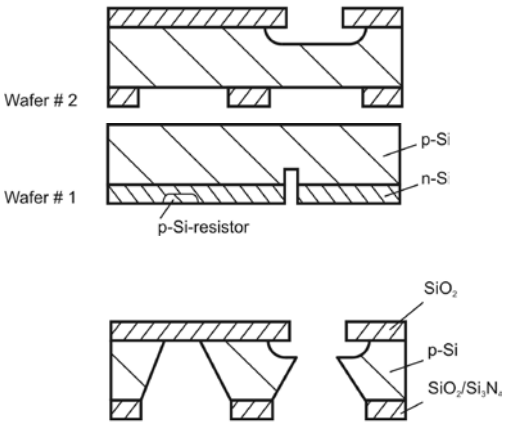

Implantation of p-Si-piezoresistors in the n-Si-epitaxial layer of a p-Si-wafer
RIE-etching

FS: Isotropic wet chemical Si-etching
BS: Anisotropic wet chemical Si-etching
(prior to this, deposition and structuring of the corresponding SiO_2/Si_3N_4 etch mask layers)

Wafer #1 and #2:
Silicon direct bonding
Anodic bonding to the pre-structured glass substrate
Etchback of the p-Si-substrate of wafer #1 to n-Si-epitaxial layer

Picture 7: Manufacturing process for the acceleration sensor

Exercise 4.10

According to ISO 286, the function of tolerance factors i is used to determine the values of the basic tolerances of qualities IT 5 … IT 18 (grades of basic tolerance) for rated dimensions of up to 500 mm. Equation $i = 0.45\sqrt[3]{D} + 0.001D$ is used to calculate tolerance factor i. Here, $D = \sqrt{D_1 D_2}$ is the geometric mean of the corresponding rated dimension range and D_1, D_2 are the range limits. For basic tolerance grades IT 5 … IT 7, it applies that

$$T_{IT5} = 7 \cdot i$$
$$T_{IT6} = 10 \cdot i$$
$$T_{IT7} = 16 \cdot i$$

(for each successive quality, the basic tolerance increases by the factor 1.6, e.g. $T_{IT12} = 160 \cdot i$).

For rated dimensions 1 … 6 mm, the following table provides basic tolerances for basic tolerance grades IT 5 … IT 7 as well as their proportion in percent of the rated dimension. The percentage in brackets refers to the geometric mean value D of the corresponding rated dimension range. It illustrates that the proportion of the tolerance rapidly increases with decreasing rated dimension. For rated dimensions lower than 1 mm, this tendency becomes stronger (see Table 1 and Picture 8).

Table 1. Basic tolerance grades IT 5 … IT 7 and their proportion in percent of the rated dimension

N mm	D mm	i µm	T_{IT5} µm	T_{IT5}/N %	T_{IT6} µm	T_{IT6}/N %	T_{IT7} µm	T_{IT6}/N %
1 … 3	1.732	0.542	4	0.13 … 0.4 (0.23)	6	0.2 … 0.6 (0.35)	10	0.33 … 1.0 (0.58)
3 … 6	4.243	0.734	5	0.08 … 0.17 (0.12)	8	0.13 ... 0.26 (0.19)	12	0.2 … 0.4 (0.28)

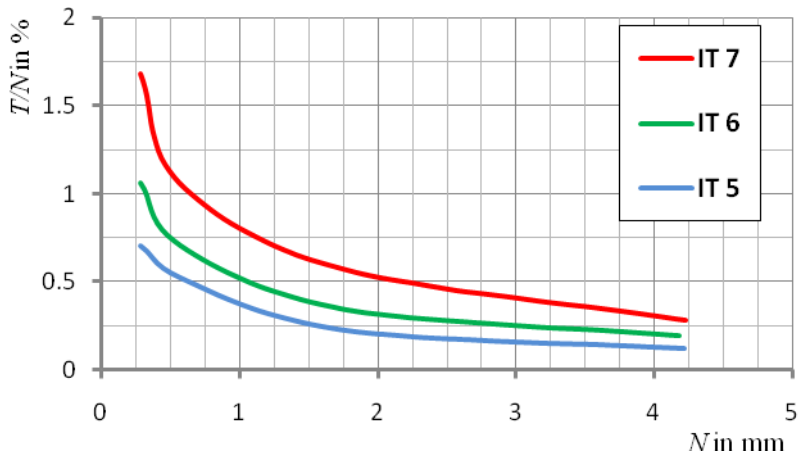

Picture 8. Basic tolerance grades IT 5 … IT 7 and their proportion in percent of the rated dimension

There is a large demand for new developments in the area of dimensioning and tolerances as well as test and measurement technology for microcomponents: Design of function-oriented tolerating basics (especially for rated dimensions smaller than 1 mm), control of existing as well as introduction of new parameters for describing microcomponent characteristics (e.g. dimensions, form deviations, waviness, roughness, three-dimensional surface parameters, structure-oriented parameters), new measuring strategies and technologies (measuring function surfaces with a resolution in the nanometer range, short measuring times, number and distribution of measuring points), standards for tolerances, measuring and control procedures.

Solutions to the exercises of chapter 5: Packaging

Exercise 5.1

Yaw rate sensor (Figure 1.7 in the book):

- electrical: - Metallization (conducting lines) of the acceleration sensors
- mechanical: - Glass substrate (mechanical carrier)
  - Thick rim of Si chip (mechanical reinforcement, bonding area to the glass substrate)
- sensorical: - Acceleration sensors
  - Oscillating mass as yaw-rate sensitive oscillating structure
- thermal: - Si-chip for heat dissipation
- protective: - Glass substrate
  - Si cover with glass seal (both for hermetic casing)

Ink-jet print head:

- electrical: - Contacting of actuator elements
- mechanical: - Casing
- sensorical: - None
- thermal: - Micro-heater for ink-jet generation
  - Ink chamber for heat loss dissipation
- protective: - Casing

Infrared bolometer focal plane array (Figures 10.2 to 10.4 in the book):

- electrical: - Bond pads
  - Contact reinforcement
  - Contact holes
- mechanical: - Carrier wafer
  - Contacting columns
- sensorical: - Bolometer pixel
- thermal: - Si wafer as heat sink
- protective: - Si carrier wafer
  - Casing

Exercise 5.2

Fixed (investment) costs FK_m for the monolithic integration amount to € 10 million and cannot be influenced. Therefore, we have to check whether and how much the unit cost VK_m can be reduced. According to equation 5.3 from the book, it applies that:

$$VK_m \le VK_h - \frac{FK_m - FK_h}{n},$$

if for an assumed number of units n the monolithic integration (index m) is more economical than the hybrid integration (index h). Applying the given values $n = 10^6$, $FK_m = 10^7$ €, $FK_h = 10^6$ €, $VK_h = 15$ €, it results that

$$VK_m \le 6 \text{ €}.$$

As casing and encapsulation cost 2 € per sensor, there remain 4 € for the monolithic production of one acceleration sensor. There are mainly two ways to reduce the current chip production cost of 10 € to 4 €:

- Increasing the yield by factor 2,5 (only possible if it is currently 40 % or below),
- Reducing the chip area to 40 % (production costs are approximately proportional to the chip area).

Exercise 5.3
Thermal adjustment of the pressure sensor in Figure 5.2 from the book using

- a fixed assembly with adjusted temperature coefficient of linear expansion: anodic bonding between Si sensor chip 1 and glass counter-body 2,
- mechanical stress decoupling by highly elastic intermediate layer: embedding the compound system of Si sensor chip 1/counter-body 2 via elastic soft glue points 3 and soft protective gel 7 in housing 4.

Exercise 5.4
Heat conduction paths from the piezoresistors

→ Si pressure plate 3 → Si sensor chip 1 (largest part of the heat dissipation),

→ Al-conducting lines 5 → insulating layer 4 → Si sensor chip 1,

→ Al-conductin lines 5 → wire bond pads 6 → contact pins 7,

→ surrounding air (mainly heat dissipation, rather seldom convection).

Exercise 5.5
Reasons for fatigue: cyclical mechanical or thermal loads
Influencing factors:
- Local stress concentration
- Surface roughness, condition
- Type of material
- Temperature, particularly temperature gradient in the material
- Material defects etc.

Reasons for delamination: Separation of composite layers due to deficient adhesion
Influencing factors:
- Cyclical mechanical or thermal loads
- Impact effect etc.

Exercise 5.6
Inertial measurands (acceleration, rotational acceleration) affect even function elements and components within hermetically sealed housings, where the impact of other disturbances can be decoupled due to the hermetical sealing. For pressure sensors, it is necessary that the respective pressure medium (e.g. air) can directly impact the sensor, which means that with that medium also disturbance variables can exercise an influence.

Solutions to the exercises of chapter 6: Function and Form Elements in Microsystem Technology

Exercise 6.1

Using equation 6.17 from the book, it applies for the eigenfrequency that

$$f_e = \frac{1}{2\pi}\sqrt{\frac{c}{m}} = \frac{1}{2\pi}\sqrt{\frac{F/y}{F/a_N}} = \frac{1}{2\pi}\sqrt{\frac{a_N}{y}}\,.$$

For the given values of rated acceleration and eigenfrequency of the movable element, it results that

$$y \le \frac{a_N}{(2\pi\, f_e)^2} = 0.65\ \mu\text{m}.$$

Exercise 6.2

Applying equation 6.55 from the book, it applies for the heat flow that moves due to heat conduction from the mirror plate to the frame that $\Phi_{thcd} = \frac{\Delta T}{R_{thcd}}$, with the thermal resistance for heat conduction being

$$R_{thcd} = \frac{s}{\lambda A}.$$

The two silicon springs with thermal resistances R_{th1}, R_{th2} act as a parallel circuit. Total thermal resistance thus becomes $R_{thtot} = \frac{R_{th1}\cdot R_{th2}}{R_{th1}+R_{th2}}$. Due to $R_{th1} = R_{th2} = R_{th}$, the result is

$$R_{thtot} = \frac{R_{th}}{2} = \frac{1000\,\mu\text{m}}{2\cdot 30\cdot 60\,\mu\text{m}^2\cdot 156\ \text{W/Km}} = 1780\ \text{K/W}.$$

The resulting heat flow is $\Phi_{thcd} = \frac{60\,\text{K}}{1780\,\text{K/W}} = 33.7\ \text{mW}.$

Exercise 6.3

a) Bulk micromachining with the oscillator moving perpendicularly to the wafer surface:

$$f_e = \frac{1}{2\pi}\sqrt{\frac{c}{m}} = \frac{1}{2\pi}\sqrt{\frac{E\cdot b\cdot h^3}{4l^3\cdot b_m l_m h\cdot\rho}} = \frac{1}{2\pi}\sqrt{\frac{E\cdot b\cdot h^2}{4l^3\cdot b_m\cdot l_m\cdot\rho}}\,.$$

With $\Delta f_e = S_h\cdot\Delta h$, it results that $\Delta f_e / f_e = \Delta h/h$, i.e. a relative thickness variation causes an identical relative variation of the oscillator's eigenfrequency (S_h is the absolute sensitivity of the initial value f_e in relation to parameter h).

b) Surface micromachining with the oscillator moving laterally in relation to the wafer surface: Thickness h does not affect the oscillator's eigenfrequency as it is not included in the equation for f_e:

$$f_e = \frac{1}{2\pi}\sqrt{\frac{c}{m}} = \frac{1}{2\pi}\sqrt{\frac{E\cdot b^3\cdot h}{4l^3\cdot b_m\cdot l_m\cdot h\cdot\rho}} = \frac{1}{2\pi}\sqrt{\frac{E\cdot b^3}{4l^3\cdot b_m\cdot l_m\cdot\rho}}\,.$$

For the relative variation of the oscillator's eigenfrequency, it then applies that $\Delta f_e / f_e = \Delta b/b$. Using the mask, it is possible to very precisely set the measure for b.

Exercise 6.4

The damping of movable micromechanical elements can be affected by gas pressure, gas type, gap distance and the structure of the oscillating plates (perforation, grooves). If the plate moves parallel to the fixed surface, the pressure in the air gap will not change. The damping effect results from the gravity forces in the fluid (slide-film damping).

If the plate moves vertically to the fixed surface, pressure will act on the gas. The gas partially escapes through the gap between movable and fixed plate and produces friction losses (squeeze-film damping). Especially when the gaps are narrow and plate frequency is high, part of the gas cannot escape from the gap and will be compressed. These two physical phenomena produce a force on the plate which can be represented as a complex expression. The real component acts as damping k_S, the imaginary component as an additional spring c_s, which changes the system's stiffness. Both effects are related to pressure and frequency. The frequency of the oscillating mass when real and imaginary force is identical is called cut-off frequency. For frequencies below cut-off the damping component is larger ($k_{eff} = k + k_s(\omega)$), for working frequencies below cut-off, the stiffness component is dominating ($c_{eff} = c + c_s(\omega)$). Typical plate dimensions in the millimetre range and typical gap distances of 1 ... 6 µm produce cut-off frequencies below 1 kHz.

For vertical plate movements, the effect of gases in narrow gaps is described as molecular or viscous flow; there is also a transitional range. In order to describe the three ranges, we use the KNUDSEN number, i.e. the ratio between gap size and mean free path of the molecules (see also Section 6.2 Fluidic Elements in the book).

Exercise 6.5

a) Applying the spring equation, it results for the stiffness acting on the probe ball that

$$c_{\mathrm{T}x,y} = \frac{F_{\mathrm{T}\max}}{s_{x,y\max}}.$$

The springs are arranged in series: both springs are loaded by the same force, the spring paths add up.

This results in $c_{\mathrm{T}x,y} = \frac{F_{\mathrm{T}\max}}{s_{x,y\max}} = \frac{F_{\mathrm{T}\max}}{s_\mathrm{F} + s_\mathrm{S}}$.

With $s_\mathrm{F} = \frac{F_{\mathrm{T}\max}}{c_\mathrm{F}}$ for the glass fibre and $s_\mathrm{S} = \frac{F_{\mathrm{T}\max} l_\mathrm{F}^{\,2}}{c_{\mathrm{S}\mathrm{rotx},y}}$ for the silicon spring (from $c_{\mathrm{S}\mathrm{rotx},y} = \frac{M}{\varphi} = \frac{F_{\mathrm{T}\max} \cdot l_\mathrm{F}}{\varphi}$ and $\varphi = \frac{s_\mathrm{S}}{l_\mathrm{F}}$), it finally results that

$$c_{\mathrm{T}x,y} = \frac{F_{\mathrm{T}\max}}{\frac{F_{\mathrm{T}\max}}{c_\mathrm{F}} + \frac{F_{\mathrm{T}\max} \cdot l_\mathrm{F}^{\,2}}{c_{\mathrm{S}\mathrm{rot}x,y}}} = \frac{1}{\frac{1}{c_\mathrm{F}} + \frac{l_\mathrm{F}^{\,2}}{c_{\mathrm{S}\mathrm{rotx},y}}} = \frac{c_\mathrm{F} \cdot c_{\mathrm{S}\mathrm{rotx},y}}{c_{\mathrm{S}\mathrm{rotx},y} + c_\mathrm{F} \cdot l_\mathrm{F}^{\,2}}.$$

b) The following table summarizes the values resulting for the spring stiffness c_F of the glass fibre and for the effective spring stiffness $c_{\mathrm{T}x,y}$ at the probe ball, based on the fibre lengths and diameters given in the task. The spring stiffness of the glass fibre is $c_\mathrm{F} = \frac{3\pi E d^4}{64\, l_\mathrm{F}^{\,3}}$.

The spring stiffness acting on the probe ball thus becomes

$$c_{\mathrm{T}x,y} = \frac{3\pi E \cdot c_\mathrm{rot} \cdot d^4}{64 c_\mathrm{rot} \cdot l_\mathrm{F}^{\,3} + 3\pi E \cdot d^4 \cdot l_\mathrm{F}^{\,2}} \text{ (see picture 9).}$$

Using $E = 75 \cdot 10^9\,\mathrm{Pa}$, c_F adopts the following values:

Table 2. Spring stiffness of the glass fibre

	c_F in N/m		
l_F	d_F = 18 µm	d_F = 40 µm	d_F = 50 µm
1 mm	1.16	28.26	69.03
2 mm	0.145	3.53	8.63
3 mm	0.043	1.05	2.55

At c_{rot}=15.3·10^{-6} Nm, the following values result for $c_{Tx,y}$:

Table 3. Spring stiffness acting on the probe

	$c_{Tx,y}$ in N/m		
l_F	d_F = 18 µm	d_F = 40 µm	d_F = 50 µm
1 mm	1.08	9.93	12.43
2 mm	0.14	1.84 2.65	
3 mm	0.04	0.68 1.02	

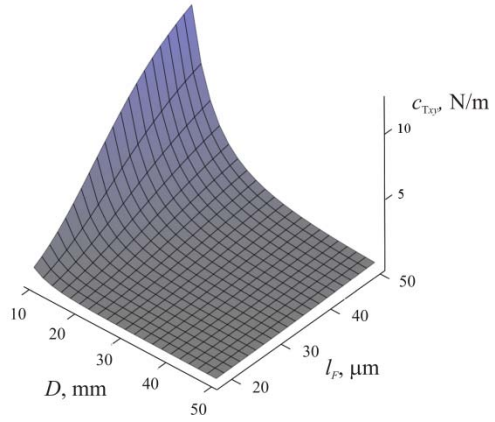

Picture 9. Spring stiffness acting on the probe ball

c) If the tactile force for s_{max} has to lie in the range of F_{Tmax} = 30 … 250 µN, using $c_{Tx,y} = \frac{F_{T\max}}{s_{\max}}$, the spring stiffness at the probe ball has to be in the range of $c_{Tx,y}$ = 1.5 … 12.5 N/m. Therefore, the fibre lengths and diameters corresponding to the shaded areas should be taken into consideration.

d) The static sagging of the sensor element due to the silicon plate's own weight is $z_{stat} = \frac{G}{c_{Sz}} = 1.32\,\mu\text{m}$. The own weight of the glass fibre can be neglected in this calculation, it amounts to less than 2 %.

e) The eigenfrequency of the sensor element in *z*-direction is $f_{ez} = \frac{1}{2\pi}\sqrt{\frac{c_{Sz}}{m_P}} = 434\,\text{Hz}$.

Exercise 6.6

The density of the water is assumed to be 1000 kg/m^3. The hydraulic diameter corresponds to the diameter of a cylindrical capillary. In this case, the WEBER number (equation 6.36 in the book) is

$$\text{We} = \frac{\rho \cdot u^2 \cdot D_H}{\sigma} = \frac{1000 \cdot (100 \cdot 10^{-6})^2 \cdot 100 \cdot 10^{-6}}{72} = 1.39 \cdot 10^{-11}.$$

The small WEBER number illustrates that - on the micro-scale - the surface tension is predominant und can therefore be used as an actuating principle.

Exercise 6.7

Here, the characteristic geometry is the diameter. Therefore, the KNUDSEN number is

$$\mathrm{Kn} = \frac{\lambda}{D_H} = \frac{6.11 \cdot 10^{-8}}{10 \cdot 10^{-6}} = 1.39 \cdot 10^{-11} = 0.00611.$$

The Knudsen number lies between 0.1 and 0.001. Therefore, we will use the continuum model with the NAVIER-STOKES equation and gliding condition at the wall.

Exercise 6.8

During the operation of the sensor, the forced convection of the thermal resistance decreases resulting in a decrease of the thermal time constant $\tau_{th} = C_{th} \cdot R_{th}$.

Exercise 6.9

The temperature at the lower side of the silicon substrate in the range of the heater structure is illustrated in the thermal equivalent circuit for the stationary case in Figure 6.17b in the book at the outgoing side of thermal resistance R_{1Si} (point $\vartheta_{\text{lower side}}$ in the picture 10). For the stationary case, we apply the simplifications provided in Example 6.6.

The total effective thermal resistance then corresponds to the series connection of $R_{1Ox} + R_{1Si}$, i.e. $R_{thcd} = (0.56 + 1.07)\ \mathrm{KW}^{-1} = 1.63\ \mathrm{KW}^{-1}$.

For a supplied heating effect of $P_{Heat} = \Phi = 1.6$ W, the resulting temperature difference in relation to the heater temperature is $\Delta T = P_{Heat} \cdot R_{thcd} = 2.5$ K.

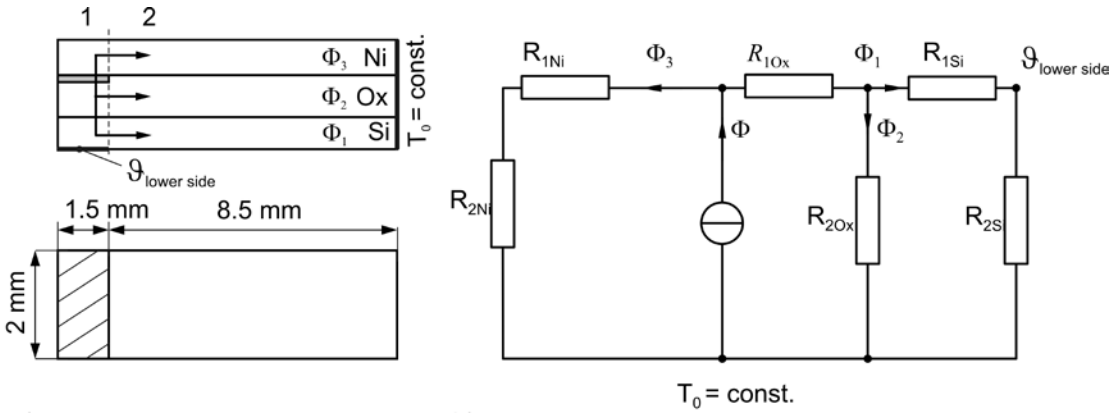

Picture 10. Thermal equivalent circuit of the air flow sensor

Solutions to the exercises of chapter 7: Sensors and Actuators

Exercise 7.1
Using the circuit in Figure 7.3a in the book, it results for the electrical side

$$\underline{V} = \underline{V_{\mathrm{c}}} + \underline{V_{\mathrm{W}}} = \frac{1}{j\omega\, C_{\mathrm{K}}}\underline{I} - \frac{A_0}{j\omega}\underline{v}$$

or transposed

$$\underline{I} = A_0 C_{\mathrm{K}}\underline{v} + j\omega\, C_{\mathrm{K}}\underline{V} = \frac{1}{Y}\,\underline{v} + j\omega\, C_{\mathrm{K}}\underline{V} \tag{15}$$

with

$$Y = \frac{1}{A_0 C_{\mathrm{K}}}. \tag{16}$$

For the mechanical right-hand side in Figure 7.3a in the book, it applies that

$$\underline{F} = \underline{F_{\mathrm{n}}} + \underline{F_{\mathrm{W}}} = \frac{1}{j\omega n_\ell}\underline{v} + \frac{A_0}{j\omega}\underline{I}$$

and inserting equation 15

$$\underline{F} = \left(\frac{1}{j\omega n_\ell} + \frac{A_0^2 C_{\mathrm{K}}}{j\omega}\right)\underline{v} + A_0 C_{\mathrm{K}}\underline{V}\,. \tag{17}$$

The term in the bracket can be expressed as

$$\frac{1}{j\omega}\left(\frac{1}{n_\ell} + A_0^2 C_{\mathrm{K}}\right) = \frac{1}{j\omega}\left(\frac{1}{n_\ell} + \frac{1}{n_{\mathrm{C}}}\right) = \frac{1}{j\omega n_{\mathrm{K}}} \tag{18}$$

with

$$n_{\mathrm{c}} = \frac{1}{A_0^2 C_{\mathrm{K}}}$$

and

$$\frac{1}{n_{\mathrm{K}}} = \frac{1}{n_\ell} + \frac{1}{n_{\mathrm{c}}}$$

or

$$n_K = \frac{n_\ell \cdot n_C}{n_\ell + n_C}\,.$$

Applying equation 16, it follows from equations 17 and 18 that

$$\underline{F} = \frac{1}{j\omega n_{\mathrm{K}}}\underline{v} + \frac{1}{Y}\underline{V}\,.$$

Equations 15 and 16 correspond to the lumped circuit in Figure 7.3b in the book or the set of equations 7.11 in the book, respectively.

Exercise 7.2
For a capacitor arrangement where one electrode is fixed and a second electrode can only move towards the other electrode (effective plate area is constant $a \cdot b$, plate distance d is variable), it results, in analogy to equation 7.14 from the book, that

$$F_{\mathrm{el}} = \frac{\partial W_{\mathrm{el}}}{\partial b} = \frac{\partial\left(\frac{V^2 C}{2}\right)}{\partial d} = \frac{V^2}{2}\,\frac{\partial C}{\partial d}$$

with

$$C = \varepsilon \frac{ab}{d}.$$

It results that

$$F_{\mathrm{el}} = -\frac{V^2}{2}\varepsilon\frac{ab}{d^2}$$

For $s = 0$ (no movement in d-direction) and $V = V_0 + \Delta V$, in analogy to equation 7.18, it results that

$$\left.\frac{\partial F_{\mathrm{el}}}{\partial V}\right|_{s=0,U=U_0} = -V_0 \cdot \varepsilon\frac{ab}{d^2} = \left.\frac{\partial Q}{\partial s}\right|_{U=U_0}.$$

It results that

$$\Delta Q = C \cdot \Delta V - \varepsilon_0 \frac{ab}{d^2} V_0 s$$

$$\Delta F = -\varepsilon_0 \frac{ab}{d^2} V_0 \Delta V + \frac{1}{n} s$$

or after the transition to harmonic, sinusoidal variables $\left(\underline{I} = j\omega\underline{Q},\ \underline{v} = j\omega\underline{s}\right)$:

$$\begin{aligned} \underline{I} &= j\omega C\underline{V} \quad - \varepsilon\frac{ab}{d^2} V_0 \underline{v} \\ \underline{F} &= -\varepsilon_0 \frac{ab}{d^2} V_0 \underline{V} \quad + \frac{1}{j\omega n}\underline{v} \end{aligned}.$$

Exercise 7.3

a), b)

If we apply supply voltage V_x to a HALL element with thickness d and have a supply current I_x, a magnetic field B_Z will induce a HALL voltage due to the HALL effect

$$V_y = \frac{B_Z R_H}{d} \cdot I_x \tag{19}$$

R_H characterizes the HALL constant

$$R_H = \begin{cases} e \cdot p & \text{für p - Si} \\ -e \cdot n & \text{für n - Si} \end{cases}, \tag{20}$$

where e is the elementary charge and p and n the charge carrier density of the electrode or the holes, respectively, in the HALL element. In addition, there is OHM's conductivity in x-direction

$$V_x = R_x \ I_x$$

As both effects occur simultaneously if current I_x flows, applying equations (19) and (20), it results that

$$I_x = \frac{1}{R_x} V_x + \frac{d}{B_Z \cdot R_H} V_y. \tag{21}$$

Due to symmetry, it has to apply at the same time in y-direction that:

$$I_y = \frac{d}{B_Z \cdot R_H} V_y + \frac{1}{R_y} V_x. \tag{22}$$

c) Equations (21) and (22) characterize two different types of transducer.

- The relationship $(V_x, I_x) \leftrightarrow (V_y, I_y)$ constitutes a reversible stationary transducer. Coupling only occurs in the case of magnetic field component $B_Z \neq 0$.

- The HALL sensor for magnetic field measuring utilizes the relationship $V_y = f(B_Z)$. This represents a parametric transducer. When measuring the voltage without current V_y ($I_y = 0$) and using equation 18, it results the relationship between voltages V_x and V_y

$$V_x = -\frac{d\,R_y}{B_Z\,R_H} V_y$$

and using equation 17

$$V_y = \frac{B_Z\,R_H}{d} \quad \frac{1}{1-\frac{R_y}{R_x}}\, I_x \tag{23}$$

equation 23 – as opposed to equation 19 – takes into account that V_x is not zero.

Exercise 7.4

The operating principle of the piezoresistive force sensor in Figure 7.25 from the book in principle corresponds to that of the piezoresistive pressure sensor in Figure 7.21 from the book, with the exception that instead of pressure p a force F acts on a cantilever beam which is clamped on one side:
Force $F \rightarrow$ mechanical strain $\varepsilon_{L,Q}$ or stress $\sigma_{L,Q} \rightarrow$ changes in relative resistance r_L ($x = 0$) or r_L $(x = \ell) \rightarrow$ change in bridge output voltage V_{out}/V_0.

According to [LENK01], it applies for the displacement of the cantilever beam which is clamped on one side that

$$\frac{s(x)}{s_0} = \left(\frac{x}{\ell}\right)^2 \left(3 - 2\,\frac{x}{\ell}\right)$$

with

$$s_0 = s(x = \ell) = \frac{\ell^3}{Ebh^3} F\ .$$

The surface stress of the cantilever beam is

$$\frac{\varepsilon_L(x)}{\varepsilon_0} = 1 - 2\frac{x}{\ell} \tag{24}$$

with

$$\varepsilon_0 = \varepsilon_L(x = 0) = 3\frac{h}{\ell^2} s_0 = 3 \cdot \frac{\ell}{Ebh^2} \cdot F\ . \tag{25}$$

Due to symmetry, it applies according to equation 23 that

$$\varepsilon_L(x = 0) = -\varepsilon_L(x = \ell) = \varepsilon_0$$

The strain-stress ratio for a wide cantilever beam ($\varepsilon_Q = 0$) is according to equation 3.8 from the book with $\sigma_Z = 0$

$$\varepsilon_L = \frac{1}{E}\sigma_L - \frac{\upsilon}{E}\sigma_Q \tag{26}$$

$$\varepsilon_Q = -\frac{\upsilon}{E}\sigma_L - \frac{1}{E}\sigma_Q = 0\,. \tag{27}$$

It directly follows from equation 27 that

$$\sigma_Q = \upsilon\sigma_L \tag{28}$$

and thus from equation 26

$$\varepsilon_L = \frac{1-\upsilon}{E}\sigma_L$$

or

$$\sigma_L = \frac{E}{1-\upsilon^2}\varepsilon_L . \tag{29}$$

Applying equations (29), (24) and (25), it results that

$$\sigma_L(x=0) = \frac{E}{1-\upsilon^2}\varepsilon_L(x=0) = \frac{E}{1-\upsilon^2}\varepsilon_0 = 3\frac{\ell}{(1-\upsilon^2)bh^2}\cdot F = -\sigma_L(x=\ell). \tag{30}$$

The further derivation follows the procedure in Example 7.8.
The output voltage of a piezoresistive full-bridge structure becomes in analogy to equation 7.122 in the book

$$\frac{V_{out}}{V_0} \approx \frac{1}{2}(r_{L1} - r_{L2}) \tag{31}$$

where r_{L1} and r_{L2} are the relative change in resistivity of the resistors at $x = 0$ or at $x = \ell$, respectively. It applies for the longitudinal resistors that:

$$r_{L1} = \pi_L \cdot \sigma_L(x=0) + \pi_Q \cdot \sigma_Q(x=0)$$
$$r_{L2} = \pi_L \cdot \sigma_L(x=\ell) + \pi_Q \cdot \sigma_Q(x=\ell)$$

and applying equations 28 and 30

$$r_{L1} = -r_{L2} = (\pi_L + \upsilon\pi_Q)\sigma_L(x=0),$$

equation 31 becomes

$$\frac{V_{out}}{V_0} = r_{L1} = (\pi_L + \upsilon\pi_Q)\cdot 3\cdot\frac{\ell}{(1-\upsilon^2)bh^2}\cdot F$$

With $\pi_L = -\pi_Q = 5 \cdot 10^{-10}$ m²/N, $\nu = 0.063$ and the given geometric dimensions, it results for this specific structure that

$$V_{out} = 10\,\mathrm{V}\cdot 4.685\cdot 10^{-10}\,\mathrm{m^2/N}\cdot 3\cdot\frac{0.5\,\mathrm{mm}}{0.996\cdot 1\,\mathrm{mm}\cdot 10^{-4}\,\mathrm{m^2}\cdot 10^{-3}\,\mathrm{N}} = 0.07\,\mu\mathrm{V}$$

This voltage is much too low for feasible technical applications which need output voltages in the mV range. This requires a sensitivity that is four orders larger. This could be achieved, for instance, by reducing cantilever thickness (the square of which is included in the output voltage) to 1 µm and the cantilever width to $^1/_{100}$.

[Lenk01] Lenk, A, Pfeifer, G., Werthschützky, R. (2001) Elektromechanische Systeme (Electromechanical Systems). Berlin: Springer.

Exercise 7.5

In the case of very small cantilever beams we have to use equation 7.126 from the book. However, - as opposed to very wide cantilever beams - there is no lateral bending in the case of very small cantilever beams. As a boundary condition, it applies for thin cantilever beams in addition to $\sigma_3 = 0$ also $\sigma_Q = 0$ instead of $\varepsilon_Q = 0$. Using equation 7.126, it then follows that

$$\pi_L\sigma_L = K_L\cdot\varepsilon_L + K_Q\varepsilon_Q$$
$$\pi_Q\sigma_L = K_Q\cdot\varepsilon_L + K_L\varepsilon_Q. \tag{32}$$

Equation 3.8 from the book results in

$$\varepsilon_L = \frac{1}{E}\sigma_L;\quad \varepsilon_Q = -\frac{\upsilon}{E}\sigma_L .$$

Inserting into equation 32, it results that

$$\pi_L = \frac{1}{E}(K_L - \nu K_Q);\quad \pi_Q = \frac{1}{E}(K_Q - \nu K_L).$$

Solving for K_L and K_Q, in analogy to Example 7.9, it results that

$$K_L = \frac{E}{1-\nu^2}\left(\pi_L + \pi_Q \cdot \nu\right); \quad K_Q = \frac{E}{1-\nu^2}\left(\pi_Q + \pi_L \cdot \nu\right).$$

As opposed to equation 7.131 from the book, the last one include the term $E/(1 - \nu^2)$ instead of $E/(1 - \nu)$. The K factors for small cantilever beams are therefore smaller by factor

$$(1 - \nu) / (1 - \nu^2) = 1/(1 + \nu) = 1/1.063 = 0.941$$

compared to wide cantilever beams. For other crystal orientations in silicon with a much larger POISSON's ratio υ (see Table 3.7 in the book), the loss in sensitivity is much higher.

Exercise 7.6

Surface and near-surface micromachining often use capacitive comb structures. A comb system (interdigital finger structure, interdigital capacitor, comb drive) consists of adjacent fixed and movable fingers, which are designed as a repetitive structure (see picture 11). The cyclically repeated section is the elementary cell.

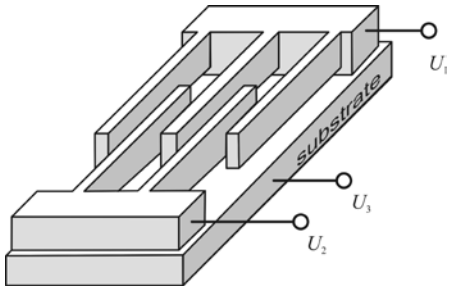

Picture 11. Comb cell

Comb cells can be used for sensoric and actuating function structure (e.g. for force generation). The capacitive sensitivities or effects, respectively, always exist in all three spatial dimensions. An elementary cell can contain up to three separate electrically controllable electrode areas.

The spring suspension defined in the design will determine the operational direction. In the operational direction, the spring suspension has the largest flexibility. In the other spatial directions, the suspension should be as stiff as possible, in order to reduce the cross-sensitivities. Operating directions can be horizontal in relation to the orientation of the bridge, horizontally transversal to the orientation of the bridge or vertical. Horizontally moved comb structures - according to Table 7.3b from the book - show a very good linearity in the overlapping range of the movement. As opposed to this, transversally moving comb cells are always non-linear, according to Table 7.3a in the book.

For horizontally moved comb cells (according to Table 7.3b,c - area variations), corresponding electrode areas are electrically connected, which means that finally there will remain only two electrodes with an active capacity, i.e. there is a parallel circuit with many small plate capacitors. This means that for small structural dimensions it is possible to generate comparatively large capacity changes $dC(x)/dx$ and therefore comparatively large forces for actuating applications

$$F_{el} = \frac{dW_{el}}{dx} = \frac{V^2}{2} \cdot \frac{dC(x)}{dx}$$

and the corresponding transformation currents for sensoric applications

$$I(t) = V_{pol} \frac{dC(x)}{dt} = V_{pol} \frac{dC(x)}{dx} \cdot \frac{dx}{dt}.$$

The change in capacity is only related to the area, but not to the electrode distance. The effect

$$F_{el} = \frac{V^2}{2} \cdot \frac{2n \cdot \varepsilon \cdot a}{d},$$

i.e. the electrostatic driving power reached by the comb drives is mainly determined by number n of the comb arms as well as comb depth a and capacitor gap d that can be achieved given the technologically feasible tolerances.

Comb cells can be used to generate comparatively large movements in the wafer plane. As opposed to plate capacitors with distance variation, it is possible to achieve a linear electromechanical transfer function.

Transversally moved comb cells (according to Table 7.3a – distance variation) constitute differential capacitors. A comb movement in the given direction produces for each comb finger and its fixed counter-electrode different, non-linear capacity functions. Measurand x produces an opposite change of both capacities, while other variables (e.g. humidity h, temperature ϑ) effect both capacities in the same direction. It applies for the two capacities of an elementary cell that

$$C_1(x) = \frac{\varepsilon ab}{d-x} = C_1 + \Delta C_1; \quad C_2(x) = \frac{\varepsilon ab}{d+x} = C_2 - \Delta C_2.$$

The differential signal $\Delta C(x) = \Delta C_1 - (-\Delta C_2)$ is measured as follows:

$$\Delta C(x) = \frac{\varepsilon ab}{d-x} - \frac{\varepsilon ab}{d+x} = C_0 \cdot \left(\frac{1}{1-\frac{x}{d}} - \frac{1}{1+\frac{x}{d}} \right), \text{ with } C_0 = \frac{\varepsilon ab}{d}.$$

A series expansion results in

$$\Delta C(x) = C_0 \left(1 + \frac{x}{d} + \left(\frac{x}{d}\right)^2 - \ldots - \left(1 - \frac{x}{d} + \left(\frac{x}{d}\right)^2 - \ldots \right) \right).$$

For small x, the series can be interrupted after the linear term:

$$\Delta C(x) \cong C_0 \left(1 + \frac{x}{d} - \left(1 - \frac{x}{d} \right) \right) = C_0 \left(\frac{2x}{d} \right).$$

The differential principle thus causes the sensitivity to double in relation to measurand x. In addition, it causes a linearization of the output signal as well as suppresses other variables. The effect becomes obvious if the output signals of both capacities are expanded in a TAYLOR series as functions of both variables (x, h):

$$C(x_0 \pm x,\, h_0 \pm h) = C(x_0,\, h_0) + \left(\pm \frac{\delta C(x_0, h_0)}{\delta x} \cdot x + \frac{\delta C(x_0, h_0)}{\delta h} \cdot h \right)$$
$$+ \frac{1}{2} \left(\frac{\delta^2 C(x_0, h_0)}{\delta x^2} \cdot x^2 \pm 2 \frac{\delta^2 C(x_0, h_0)}{\delta x \cdot \delta h} x \cdot h + \frac{\delta^2 C(x_0, h_0)}{\delta h^2} h^2 \right).$$

It results for the differential signal ΔC that

$$\Delta C = C(+x,h) - C(-x,h) = 2 \left(\frac{\delta C(x_0, h_0)}{\delta x} \cdot x + \frac{\delta^2 C(x_0, h_0)}{\delta x \cdot \delta h} \cdot x \cdot h \right).$$

The linear term of variable h and the purely square terms do not have any effect on differential signal ΔC. What remains is the effect of the mixed square term.

Figure 8.8 in the book shows that the output characteristic of a micromechanical actuator for a differential capacitor operation is linearized by the polarisation voltage. Figure 8.9 in the book illustrates the doubling of the sensitivity for a micromechanical sensor for a differential capacitor operation. The difference between capacitive transformation currents due to capaci-

tances C_1, C_2 and the subsequent current-voltage-transformation generates the output signal of the sensor.

Differential capacitors are also used for sensors in closed-loop operations in order to measure capacity and - at the same time - electrically generate compensation forces.

Exercise 7.7

a) The limit acceleration a_G has to produce a displacement of the mass by 1 µm, i.e. acceleration force F_a has to compensate the spring's restoring force at a displacement of 1 µm: $F_a = F_F$ with $F_a = m \cdot a$ and $F_F = c_{tot} \cdot x$. It results that

$$a_G = \frac{c_{tot} \cdot x}{m} = \frac{2c_S \cdot x}{\rho h d^2} = \frac{2Ehb^3}{l^3 \rho h d^2} = \frac{2Eb^3}{l^3 \rho d^2}.$$

Spring stiffness c_{tot} thereby results from the parallel connection of two S-springs, whose spring stiffness c_S can be calculated according to equation (6.29) from the book.
From the given numerical values, it results that: mass $m = 92 \cdot 10^{-11}$ kg, spring stiffness $c_{tot} = 50 \cdot 10^{-3}$ N/m, $a_G \geq 54.4$ m/s^2 ($\cong 5.54 \cdot g$).

b) At $a_G = 54.4$ m/s^2, the contact force is $F_K = 0$.

c) The mounting position of the sensors determines whether and how the own weight of the mass ($G = mg = 9 \cdot 10^{-9}$ N) has to be included into the calculation of a_G: $a_{Gmax} = 64$ m/s^2, $a_{Gmin} = 44$ m/s^2.

d) In order to produce a contact force $F_K \geq 1$ µN, we need an acceleration $a = \frac{F_{close} + F_K}{m}$, with $F_{close} = c_{tot} \cdot x = 50 \cdot 10^{-9}$ N.
Applying the given numerical values, it results that $a = 1141$ m/s$^2 \cong 116$ g.

e) According to equation 7.57 from the book $F_{el} = \frac{V^2}{2} \frac{dC(x)}{dx} = \frac{V^2}{2} \frac{2n\varepsilon t}{d}$.
The voltage has to be large enough to produce a displacement of $x = 1$ µm. That requires a force of $F_{el} = F_{close} = c_{tot} \cdot x = 50 \cdot 10^{-9}$ N. With number of comb arms $n = 8$, electrode distance $d = 1$ µm, structure depth $t = 10$ µm, it results that $V = \sqrt{\frac{c_{tot} x \cdot d}{n \cdot \varepsilon \cdot t}} = 8.4$ V.

f) If contact force $F_K \geq 1$ µN is to be produced during the self-test, the required voltage increases to $V_{self\ test} = 38.5$ V.

Exercise 7.8

For determining the relation of displacement angle φ of a 1D torsional mirror (see picture 12) and voltage V at the electrode surfaces, we can use the torque equilibrium $M_{mech} = c_\varphi \cdot \varphi = M_{el}$: $\varphi = M_{el} / c_\varphi$.

The spring stiffness of the torsional spring is $c_\varphi = 2 \cdot I_t \cdot G / L$, with I_t being the torsional resistance and G the shear modulus. For a torsional spring with a rectangular cross-section $w \times h$, it results that $I_t = w \cdot h^3 \cdot k_1$. Depending on the ratio w/h, factor k_1 can assume values of $k_1 = 0.140 \ldots 0.333$. For trapecoidal spring cross-sections (fabricated by wet chemical etching), the term for the torsional resistance would be much more complex. The difference in I_t is comparatively small if you change width w but keep thickness h constant, for instance. Therefore it is usually sufficient to consider the rectangular cross-section.
In the following, we will calculate the electric torque for the case represented in the picture 12. That means that only the electrode under the right side of the mirror plate is controlled by voltage V.

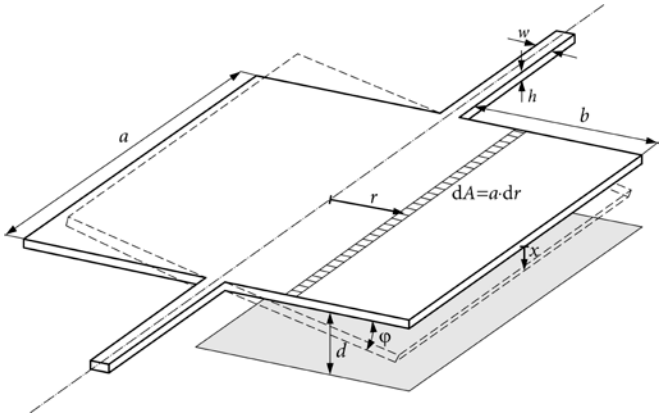

Picture 12. 1D torsional mirror

It applies for the electrostatic force acting on the movable mirror plate that

$$F_{\mathrm{el}} = \frac{\mathrm{d}W_{\mathrm{el}}}{\mathrm{d}x} = \frac{V^2}{2} \cdot \frac{\mathrm{d}C}{\mathrm{d}x}.$$

The capacity function $C(x)$ for the right side of the plate capacitor is

$$C(x) = \varepsilon \frac{a \cdot b}{d - x}, \text{ i.e. } \frac{\mathrm{d}C}{\mathrm{d}x} = \varepsilon \frac{a \cdot b}{(d - x)^2}.$$

Note: Force F_{el} strives to increase the capacity, i.e. to reduce plate distance d. As the direction of the electrostatic force acting on the electrodes coincides with the direction of the distance reduction, it applies that $-\mathrm{d}d = \mathrm{d}x$ and $\mathrm{d}C/\mathrm{d}x = -\mathrm{d}C/\mathrm{d}d$.

If the mirror plate is displaced due to the acting force ($\varphi > 0$), the actual distance $x = r \cdot \tan\varphi$ between movable mirror plate and base electrode decreases depending on distance r to the rotational axis (depending on whether we take the fixed base electrode or the movable mirror electrode as reference base, we can also write $x = r \cdot \sin\varphi$ instead of $x = r \cdot \tan\varphi$. For the angles we look at ($\varphi \leq 10°$), it is sufficiently precise to apply $\sin\varphi \cong \tan\varphi$, therefore the distinction is not critical).

We arrive at the electric torque M_{el} acting on the right side of the mirror plate if we sum up all partial torques $\mathrm{d}M_{\mathrm{el}}$ that act on the narrow strips with area $\mathrm{d}A = a \cdot \mathrm{d}r$ and that each have a distance to the base electrode of $d - x = d - r \cdot \tan\varphi$.

For each partial torque, it applies that $\mathrm{d}M_{\mathrm{el}} = \mathrm{d}F_{\mathrm{el}} \cdot r$.

The summation is carried out within the limits of $r = 0 \ldots b$.

With

$$\mathrm{d}F_{\mathrm{el}} = \frac{V^2}{2} \cdot \varepsilon \frac{a \cdot \mathrm{d}r}{(d - x)^2} = \frac{V^2}{2} \cdot \varepsilon \frac{a \cdot \mathrm{d}r}{(d - r \cdot \tan\varphi)^2}$$

it results that $M_{\mathrm{el}} = \int_{r=0}^{r=b} \mathrm{d}M_{\mathrm{el}} = \frac{V^2 \cdot \varepsilon \cdot a}{2} \int_{r=0}^{r=b} \frac{r \cdot \mathrm{d}r}{(d - r \cdot \tan\varphi)^2}$.

Substituting $z = d - r \cdot \tan\varphi$, it results that $\mathrm{d}r = -\mathrm{d}z/\tan\varphi$ and subsequently

$$M_{\mathrm{el}} = \frac{V^2 \cdot \varepsilon \cdot a}{2} \int \frac{d - z}{(-z^2 \cdot \tan^2\varphi)} \mathrm{d}z = \frac{V^2 \cdot \varepsilon \cdot a}{2 \cdot \tan^2\varphi} \int \left(\frac{1}{z} - \frac{d}{-z^2} \right) \mathrm{d}z.$$

$$M_{\mathrm{el}} = \frac{V^2 \cdot \varepsilon \cdot a}{2 \cdot \tan^2\varphi} \cdot \left(\ln z + \frac{d}{z} \right) = \frac{V^2 \cdot \varepsilon \cdot a}{2 \cdot \tan^2\varphi} \cdot \left[\ln(d - r \cdot \tan\varphi) + \frac{d}{d - r \cdot \tan\varphi} \right]_0^b$$

$$M_{\mathrm{el}} = \frac{V^2 \cdot \varepsilon \cdot a}{2 \cdot \tan^2\varphi} \cdot \left[\ln(1 - \frac{b}{d} \cdot \tan\varphi) + \frac{b \cdot \tan\varphi}{d - b \cdot \tan\varphi} \right].$$

With $A = \frac{b \cdot \tan\varphi}{d}$, it results that

$$M_{el} = \frac{V^2 \cdot \varepsilon \cdot a}{2 \cdot \tan^2\varphi} \cdot \left[\ln(1-A) + \frac{A}{1-A} \right].$$

Note: For static displacement, it will apply that $b \cdot \tan\varphi < d/3$ due to the pull-in effect. Therefore, A will lie in the range of $A = 0 \ldots 0.333$. For resonant operation, the pull-in effect does not play any roll. In that case, we have to include the relation $\varphi_{res} \cong Q \cdot \varphi_{stat}$).

It finally results that

$$\varphi = \frac{M_{el}}{c_\varphi} = \frac{V^2 \cdot \varepsilon \cdot a}{c_\varphi \cdot 2 \cdot \tan^2\varphi} \cdot \left[\ln(1-A) + \frac{A}{1-A} \right] = \frac{V^2 \cdot \varepsilon \cdot a \cdot L}{4 \cdot w \cdot h^3 k_1 \cdot G \cdot \tan^2\varphi} \cdot \left[\ln(1-A) + \frac{A}{1-A} \right].$$

Stating the relation of angle and voltage $\varphi = f(V)$ is not trivial, as there are several steady states for a given voltage V. Reversely it is possible though to unambiguously determine the voltage V required for a given displacement angle φ:
The ratio voltage-angle $V(\varphi)$ is

$$V(\varphi) = \sqrt{\frac{4 \cdot w \cdot h^3 k_1 \cdot G \cdot \varphi \cdot \tan^2\varphi}{\varepsilon \cdot a \cdot L \cdot \left[\ln(1-A) + \frac{A}{1-A} \right]}} = \sqrt{\frac{4 \cdot I_t \cdot G \cdot \varphi \cdot \tan^2\varphi}{\varepsilon \cdot a \cdot L \cdot \left[\ln(1-A) + \frac{A}{1-A} \right]}} = \sqrt{\frac{2 \cdot c_\varphi \cdot \varphi \cdot \tan^2\varphi}{\varepsilon \cdot a \cdot \left[\ln(1-A) + \frac{A}{1-A} \right]}}.$$

For a square mirror plate (mirror length $a = 2 \cdot b$), it results that

$$V(\varphi) = \sqrt{\frac{2 \cdot w \cdot h^3 k_1 \cdot G \cdot \varphi \cdot \tan^2\varphi}{\varepsilon \cdot b \cdot L \cdot \left[\ln(1-A) + \frac{A}{1-A} \right]}} = \sqrt{\frac{2 \cdot I_t \cdot G \cdot \varphi \cdot \tan^2\varphi}{\varepsilon \cdot b \cdot L \cdot \left[\ln(1-A) + \frac{A}{1-A} \right]}} = \sqrt{\frac{c_\varphi \cdot \varphi \cdot \tan^2\varphi}{\varepsilon \cdot b \cdot \left[\ln(1-A) + \frac{A}{1-A} \right]}}.$$

Example: $\varphi(V)$ characteristic, analytically calculated with MathCad (see picture 13)
a = 4 mm, b = 2 mm, spring length L = 1.9 mm, spring thickness h = 20 µm, spring width w = 40 µm, electrode base distance d = 280 µm, controlling voltage V = 0 … 550 V.

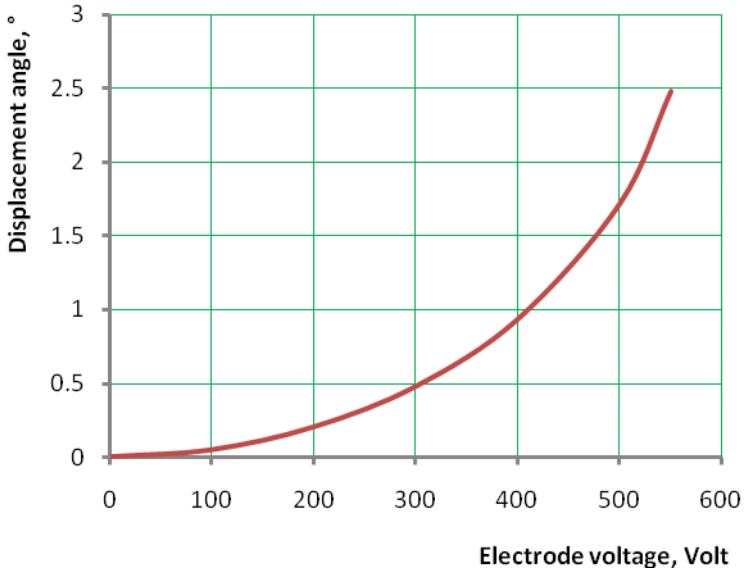

Picture 13. $\varphi(V)$ characteristic

Function $M_{el} = f(\varphi)$ is not defined for $\varphi = 0$. The effective torque at $\varphi = 0$ can be derived from the effect on the non-displaced mirror plate ($\varphi = 0$, $x = 0$), for which it applies that

$F_{el} = \frac{dW_{el}}{dx} = \frac{V^2}{2} \cdot \frac{dC}{dx} = \frac{V^2}{2} \cdot \varepsilon \frac{a \cdot b}{d^2}$. This force is applied at the centre of gravity of the right-hand mirror plate, i.e. at distance $b/2$ to the rotational axis:

$$M_{el} = F_{el} \cdot \frac{b}{2} = \frac{V^2}{2} \cdot \varepsilon \frac{a \cdot b}{d^2} \cdot \frac{b}{2} = \frac{V^2 \cdot \varepsilon \cdot a \cdot b^2}{4 \cdot d^2} \quad .$$

For a square mirror plate $a = 2 \cdot b$, it results that $M_{el} = \frac{V^2 \cdot \varepsilon \cdot b^3}{2 \cdot d^2}$.

Exercise 7.9

a) The presented frame of the approach opening is complemented with a u-shaped PMMA „light conductor" that coincides with the frame. Its opening faces the torsional mirror. The laser beam is coupled to the u-shaped light-conducting PMMA frame und led to a photo sensor that is situated at the front of the PMMA frame. When a flying object interrupts the light curtain produced by the laser at any point, the light signal at the photo sensor will be interrupted too.
In order for the laser beam to hit the flying object at least once, the minimum sampling rate has to be $f_{sampling} \geq \frac{1}{2\Delta t}$ with $\Delta t = \frac{l}{v} = \frac{5\,\text{cm}}{50\,\text{km/h}} = 3.6\ \text{ms}$.
It results that $f_{sampling} \geq 140\,\text{Hz}$.
In order to increase detection probability, we use $f_e \cong 300$ Hz as the eigenfrequency of the resonance operated micromechanical torsional mirror.

b) The distance between mirror and approach opening has to be
$L = \frac{25\,\text{cm}}{\tan\alpha_{opt}} = \frac{25\,\text{cm}}{\tan(2\alpha_{mech})} = \frac{25\,\text{cm}}{\tan 25^\circ} = 53.6\,\text{cm}$.

c) The edge length $2 \cdot b$ of the square mirror has to be larger than the diameter of the laser beam, e.g. $A_{mirror} = 4 \times 4\ \text{mm}^2$ (selected).

d) Minimum thickness D of the mirror wafer results from summing up electrode base distance and mirror thickness: $D = d + h$.
Electrode base distance d has to be sufficiently large for the fully displaced mirror plate not to hit the counter-electrode: $d > b \cdot \tan(\alpha_{mech})$. With $b = 2$ mm and $\alpha_{mech} = 12.5\,°$, it results that $d > 443\ \mu$m. Selected: $d = 450\ \mu$m. Mirror thickness h results from solution e).

e) Using the equation for the eigenfrequency of the torsional mirror
$$f_e = \frac{1}{2\pi}\sqrt{\frac{c_\varphi}{J}} = \frac{1}{2\pi}\sqrt{\frac{2 \cdot G \cdot I_t}{l \cdot J}}$$
we arrive at length l of a torsional spring
$$l = \frac{2 \cdot G \cdot I_t}{4 \cdot \pi^2 \cdot J \cdot f_e^{\,2}}.$$
Inserting into this equation the respective relations for I_t and J and using $I_t = w \cdot h^3 \cdot k_1$, $J = \frac{m}{12}(h^2 + 4 \cdot b^2) = \rho \cdot 4 \cdot b^2 \cdot h(h^2 + 4 \cdot b^2)$, $w/h = 2$, $k_1(w/h = 2) = 0.229$ and $4 \cdot b^2 >> h^2$ it results that
$$l = 2.177 \cdot 10^{-3} \cdot \frac{G}{\rho} \cdot \frac{w^3}{f_e^{\,2} \cdot b^4}.$$
Here, c_φ is the spring stiffness for torsion, J the mass moment of inertia, $2 \cdot b$ the edge length of the mirror, h the thickness of mirror and torsional spring, $w = 2 \cdot h$ the width of

the torsional spring, G the shear modulus, m the mirror mass, ρ the density and I_t the torsional resistance. .
Applying the values $G(w/h = 2) = 55$ GPa, $b = 2$ mm, $\rho = 2330$ kg/m^3 and $f_e = 300$ Hz, for the free design parameters spring length l and spring width w, it results that ratio $l/\text{mm} = 35.7 \cdot 10^{-6} \cdot (w/\mu\text{m})^3$, i.e. $l \sim w^3$,

Table 4. Micromirror design parameters

w/µm	l/mm
20	0.285
30	0.964
34	1.40
36	1.67
38	1.96
40	2.28
60	7.71

The values preferred due to technological reasons are highlighted in grey. We select $w = 40$ µm, which results in $h = 20$ µm, and for thickness D of the mirror wafer (see task d), the result is $D \geq 470$ µm.

Torque equilibrium $M_{mech} = M_{el}$ results in voltage V, that is required to statically displace the square mirror by $\alpha_{stat} = \alpha_{mech}$

$$V(\alpha) = \sqrt{\frac{2 \cdot w \cdot h^3 k_1 \cdot G \cdot \alpha \cdot \tan^2\alpha}{\varepsilon \cdot b \cdot l \cdot \left[\ln(1-A) + \frac{A}{1-A}\right]}} \qquad \text{with } A = \frac{b \cdot \tan\alpha}{d}$$

(Note: See also solution 7.8. In Exercise 7.9, displacement angle and spring length have different denominations: displacement angle α instead of φ, spring length l instead of L).

Due to $\alpha_{res} = Q \cdot \alpha_{stat}$ and $Q = 100$, the above equation has to solved for an angle of $\alpha_{stat} = \alpha_{mech} = 0.125$ °.
The values of $\alpha = 0.125$ °, $w = 40$ µm, $h = 20$ µm, $k_1 = 0.229$, $G = 55$ GPa, $b = 2$ mm, $d = 450$ µm, $L = 2.28$ mm, $\varepsilon = 8.8542 \cdot 10^{-12}$ As/Vm result in
$V(\varphi_{stat} = 0.125\ °) \cong 208$ V.
Regarding the electrode base distance, we have to take into account the difference between static and dynamic operation of the micromechanical torsional mirror (see also Exercise 7.8): For a static displacement, $b \cdot \tan\alpha < d/3$ due to the pull-in effect. Therefore, it applies that $A \leq 0.333$.
During resonant operation of the mirror, the pull-in effect does not play any role. In that case, A usually assumes very small values. For the electrode base distance d, we have to take into account the relation $\varphi_{res} \cong Q \cdot \varphi_{stat}$ though.
With the calculated or selected values for b, l, h, w, V, the requirements regarding eigenfrequency and displacement angle are met.

f) The speed of the flying object determines according to solution a) the required minimum sampling frequency and thus the necessary eigenfrequency of the mirror.

g) If we want to detect the flight direction in addition to the passing of a flying object, we could arrange two of the approach openings represented in Figure 7.27 one after the other.

Exercise 7.10

Retaining force F results from the electrostatic force F_{el} generated by the drive, minus the restoring force F_F of the springs:

$$F = F_{el} - F_F .$$

Using the given values for the number of comb arms n = 40, effective length of the capacitor plates L = 200 µm, wafer thickness as well as plate width h = 50 µm, plate distance in steady position d_0 = 9 µm, shift path to end stop u = 7 µm, operating voltage V = 50 V, spring constant c = 18 N/m and ε_0 = $8.85 \cdot 10^{-12}$ As/Vm, the following equations and numerical values result:

Electrostatic force (plate capacitor) $F_{el} = \frac{\varepsilon_0 A}{2d^2} \cdot V^2$.

The effective capacitor area is $A = n \cdot L \cdot h = 4 \cdot 10^{-7}\,\mathrm{m}^2$ and the plate distance at end position is

$$d = d_0 - u = 2 \cdot 10^{-6}\,\mathrm{m} .$$

Therefore, it results that F_{el} = 1.48 mN. The restoring force of both springs is

$$F_F = 2 \cdot c \cdot u = 0{,}25\ \mathrm{mN} .$$

The retaining force is F = 1.23 mN.

Exercise 7.11

a) The mass is suspended above cantilever springs. Three cantilevers with stiffness c are arranged parallel, and this arrangement comprises four pairs connected in series. Total stiffness therefore is as follows:

$$\frac{1}{c_{1/4}} = \frac{1}{3c} + \frac{1}{3c}; \quad c_{1/4} = \frac{3}{2}c$$

$$c_{tot} = 4\frac{3}{2}c = 6c$$

In each case, one cantilever spring is bent in an s-shape.
Spring stiffness of a cantilever spring with height h and width b, being bent by width b in a plane:

$$c = \frac{E_x\, h\, b^3}{l^3}$$

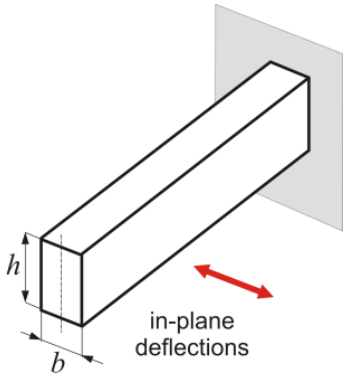

Picture 14. In-plane deflection of cantilever

Using the equation of the eigenfrequency of the structure

$$f_0 = \frac{1}{2\pi}\sqrt{\frac{c_{ges}}{m_1 + m_2}}$$

and applying transformations, the required cantilever length becomes

$$l = \sqrt[3]{\frac{3E_x b^3 h}{2\pi^2 f_0^2 (m_1 + m_2)}}.$$

Numerical value: l = 259.4 µm.

b) Applying $W_{\mathrm{el}} = \frac{1}{2} C V^2$ and $C = \varepsilon_0 \frac{(b + q_x)h}{d}$, it results for the electrostatic force that

$$F_{\mathrm{el}} = \frac{\mathrm{d}W_{\mathrm{el}}}{\mathrm{d}q_x} = \frac{\mathrm{d}}{\mathrm{d}q_x}\left(\frac{\varepsilon_0 V^2 h(b_{\ddot{u}} + q_x)}{2d}\right) = \frac{\varepsilon_0 V^2 h}{2d}.$$

Each finger of the comb drive at the seismic mass has two electrode gaps. The total force results therefore from multiplying by 2n. Two comb drives with 30 fingers each act in one direction.

The mechanical spring force is $F_{\mathrm{Spring}} = 6 c q_x$. The equilibrium of forces can be used to derive the static displacement:

$$F_{\mathrm{Spring}} = 2 \cdot 2n F_{\mathrm{el}}$$

$$6 c q_x = 4n \frac{\varepsilon_0 V^2 h}{2d}$$

$$q_x = n \frac{\varepsilon_0 V^2 h}{3 d c}.$$

At 5 Volt, the static displacement is 0,73 nm.

c) If damping is weak, the oscillation amplitude increases in case of resonance by the resonance quality factor. Micromechanical structures are mainly damped by the surrounding gas. The pressure-related dynamic viscosity can be used to influence the damping of the structure. Reducing the pressure in the sensor housing can be used to increase the mechanical quality.

d) $F_{\mathrm{C}} = 2 m_2 \Omega v$, with $v = \dot{q}_x = \hat{q}_x \omega_{01} \cos(\omega_{01} t)$

$$c_2 = \omega_{02}^2 m_2$$

$$q_y = \frac{F_{\mathrm{C}}}{c_2} = \frac{m_2 \Omega \hat{q}_x \omega_{01} \cos(\omega_{01} t)}{\omega_{02}^2 m_2}$$

with $\omega_{01} = \omega_{02} = \omega_0$ results $q_y = \frac{\Omega \hat{q}_x \cos(\omega_0 t)}{\omega_0}$

$$q_y(nT) = \frac{\Omega \hat{q}_x}{\omega_0}.$$

Taking into account a resonance quality factor of 1000, at 200 °/s the amplitude of the detection movement of the secondary oscillator amounts to approximately 1.11 µm.

e) The two capacities are measured differentially (see also Solution 7.6). The capacity is calculated as follows:

$$C = \frac{\varepsilon_0 bh}{d - q_y} - \frac{\varepsilon_0 bh}{d + q_y} = C_0 \left(\frac{1}{1 - \frac{q_y}{d}} - \frac{1}{1 + \frac{q_y}{d}} \right), \text{ with } C_0 = \frac{\varepsilon_0 bh}{d}$$

$$= C_0 \left(1 + \frac{q_y}{d} + \left(\frac{q_y}{d} \right)^2 - \ldots - \left(1 - \frac{q_y}{d} + \left(\frac{q_y}{d} \right)^2 - \ldots \right) \right).$$

For small q_y, it results that

$$C = C_0 \left(2 \frac{q_y}{d} \right); \; S = \frac{\mathrm{d}C}{\mathrm{d}q_y} = 2 \frac{C_0}{d}.$$

For n = 20 fingers, the capacity change is 0.57 pF/µm. Taking into account the results in Exercise d), it becomes 3.16 fF/°/s.

f) A direct voltage (polarization voltage V_{pol}) over the detection electrodes can be used to affect the mechanical stiffness of the secondary oscillator (c_2). For small displacements, the following electrostatic force applies:

$$F_{\mathrm{el}} = \frac{V_{\mathrm{pol}}^2}{2} \varepsilon \cdot A \cdot \left(\frac{1}{(d - q_y)^2} - \frac{1}{(d + q_y)^2} \right).$$

It opposes the spring force:

$$F_{\mathrm{tot}} = c_2 \, q_y - F_{\mathrm{el}}.$$

The stiffness is defined as a derivation of the force after the displacement:

$$\frac{\mathrm{d}}{\mathrm{d}\, q_y} F_{\mathrm{tot}} = c_2 - \varepsilon \, A V_{\mathrm{pol}}^2 \left[\frac{1}{(d + q_y)^3} + \frac{1}{(d - q_y)^3} \right]$$

and, for $q_y \rightarrow 0$, it results that:

$$\lim_{q_y \to 0} \left(\frac{\mathrm{d}}{\mathrm{d}\, q_y} F_{\mathrm{tot}} \right) = c_2 - \frac{2 \varepsilon \, A V_{\mathrm{pol}}^2}{d^3}.$$

The equation shows that the resulting stiffness can be reduced by using a polarization voltage. The eigenfrequency of the secondary oscillation can be dimensioned slightly higher than the primary frequency. Using a polarization voltage, this frequency can subsequently be adjusted.

Exercise 7.12

a) The torque results from summing up all partial torques M_k, that have been produced by the electrodynamic force acting on the individual conductors k (k = 1…n). For the partial torques, it applies that

$$M_k = F_k \cdot r_k = I \cdot B_k \cdot l_k \cdot r_k.$$

Here, r_k states the distance of a conductor to the rotational axis of the movable element. B_k is the value of the current density and l_k the length of the conductor, related to the x-coordinate of k (see figure). The current density is assumed to be constant along a conductor and over the conductor's width. For a symmetric current density distribution and a symmetric orientation of the movable element in the air gap, the total torque is

$$M_{\text{tot}} = 2 \cdot \sum_{k=1}^{n} M_k \,,$$

where n is the number of circuit loops in the planar coil.

Using the horizontal projection of the mirror plate and planar coil, we can derive the following values:

- Conductor width $b \le 50$ µm, as: width of torsion bands = 50 µm.
- Number of circuit loops: $n = 2$ mm/b
- Conductor height $h = 2$ µm
- OHM's resistance of planar coil: $R = \rho \cdot \frac{l_{\text{tot}}}{A} = \frac{\rho \cdot n \cdot 2 \cdot (D_{\text{m}} + L_{\text{m}})}{b \cdot h}$.

Applying the equations for the electrodynamically generated torques to the current situation, we arrive at $M_{\text{tot}} = 2 \cdot n \cdot I \cdot B \cdot L_{\text{m}} \cdot \frac{D_{\text{m}}}{2} = n \cdot I \cdot B \cdot L_{\text{m}} \cdot D_m$.

Inserting the given values $L_{\text{m}} = 14$ mm, $D_{\text{m}} = 4$ mm, it results that for a required torque $M_{\text{tot}} = 5.6 \cdot 10^{-6}$ Nm the product has to be $n \cdot I = 0.4$ A.
For $b_{\text{max}} = 50$ µm (width of torsion band) and $n \cdot b = 2$ mm, the number of circuit loops becomes $n = 40$, and consequently $I = 10$ mA (current density 100 A/mm^2).

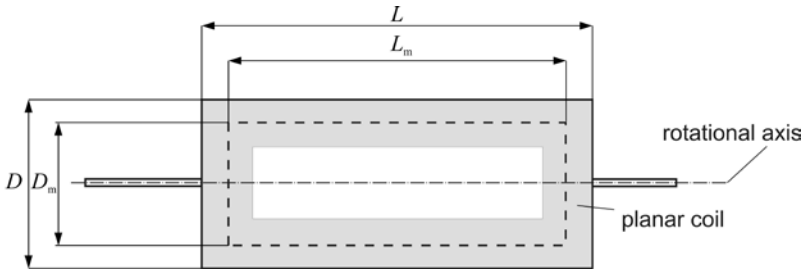

Picture 15. Planar coil

b) Using $R = \rho \cdot \frac{l_{\text{tot}}}{A} = \frac{\rho \cdot n \cdot 2 \cdot (D_{\text{m}} + L_{\text{m}})}{b \cdot h}$, the OHMic resistance of the planar coil at $\rho_{\text{Al}} = 0.028\ \Omega\text{mm}^2/\text{m}$ becomes $R = 403.2\ \Omega$.
OHMic power dissipation thus becomes $P = I^2 \cdot R = 40.32$ mW. The expected temperature increase is calculated using

$\Delta T = P \cdot R_{\text{th}} = \frac{I^2 \cdot R}{\alpha_{\text{K}} \cdot A}$ with $A = 2 \cdot D \cdot L = 192$ mm^2 and $\alpha_{\text{K}} = 10$ W/m^{2}K and becomes

$\Delta T = 21$ K.

c) No. From $\Delta T = P \cdot R_{\text{th}} = \frac{I^2 \cdot R}{\alpha_{\text{K}} \cdot A} = \frac{I^2 \cdot \rho \cdot 2 \cdot n(D_{\text{m}} + L_{\text{m}})}{\alpha_{\text{K}} \cdot A \cdot b \cdot h}$, it follows due to $b = \frac{2\,\text{mm}}{n}$ that

$\Delta T = \frac{I^2 \cdot \rho \cdot 2 \cdot n^2 (D_{\text{m}} + L_{\text{m}})}{\alpha_{\text{K}} \cdot A \cdot 2\,\text{mm} \cdot h}$.

Using the known numerical values, it results that $\Delta T / \text{K} = 131.25 \cdot (I / \text{A})^2 \cdot n^2$ and due to $n \cdot I = 04$ A, it follows that $\Delta T / \text{K} = 131.25 \cdot 0.16 = 21$ K (see above), which means independently of the selected parameters I, n.

c) If the distance between circuit loops of the planar coils has be 5 µm each and the number of circuit loops remains constant at $n = 40$, the conductor will become smaller than $b = 50$ µm. This means that R and consequently P and ΔT will increase.
An alternative would be to retain width $b = 50$ µm and to decrease the number of circuit loops to approximately $n = 36$. This way, the current would have to be increased to $I = 11.11$ mA in order to generate the same torque. The OHMic resistance would decrease to 363 Ω. The OHMic power dissipation would amount to $P = I^2 \cdot R \cdot = 44.8$ mW, i.e. ΔT would also increase.

Exercise 7.13

As an example for both actuator principles, we can use a micro-mirror with distance variation. We will present the corresponding advantages and disadvantages:

Table 5. Advantages and disadvantages of electrostatic and electrodynamic actuation principles

Micro-mirror, electrostatic drive (see Table 7.2, Figure 6.18 in the book)	**Micro-mirror, electrodynamic drive** (see Figures 7.10, 7.11 in the book)
Pros: - Small dimensions, resulting in large eigenfrequency - Capacitive localization is possible - Voltage-controlled **Cons:** - Only attracting forces possible - Damping in the air gap strongly non-linear - Electric driving torque depends on the square of the voltage. This function and its inverse cannot be continuously differentiated and have points of discontinuity - Controllability depends on mirror position - Controllability lost in the range of maximum displacement	**Pros:** - Damping can be assumed to be constant (no gap) - Force in the homogenous magnetic field is proportional to the current. Attracting and repulsive forces can be generated. - The generated torque depends only on the angle; it can be considered to be constant for small displacements - The magnetic driving torque can be affected from the outside by changing the magnetic flux density **Cons:** - Large dimensions due to planar coil on movable area - Heat dissipation from planar coil

Regarding control technology, the advantages of the electrodynamic driving principle prevail. A non-linear control of the electrostatic actuator is possible if all non-linear relations are exactly known (damping, torsional spring, characteristic voltage-angle).

Solutions to the exercises of Chapter 9: Effect of Technological Processes on Microsystem Properties

Exercise 9.1

Material parameters: • YOUNG's modulus • POISSON's ratio • Conductivity of bulk Si • Conductivity of poly-Si • Temperature coefficient of linear expansion of the Si chip • Temperature coefficient of linear expansion of the glass substrate	**Process parameters:** • Orientation of etch mask edges • Wafer orientation • Doping of Si chip • Poly-Si deposition • Anodic bonding Si-chip/glass substrate
Geometric parameters: • Thickness of the oscillating mass • Width of the oscillating mass • Length of the oscillating mass • Spring width of the oscillating mass • Spring length of the oscillating mass • Spring thickness of the oscillating mass • Width, thickness, length of the poly-Si acceleration sensor structure • Chip dimensions	**Process parameters:** • Etching time • Etching temperature • Temperature at the anodic bonding • Temperature and duration of poly-Si deposition • Temperature, pressure and duration of the metallization evaporation

Exercise 9.2

Plate thickness becomes uncritical when according to Table 9.3 or equation 9.26 from the book, respectively, it applies that

$$u\left(FP_{\mathrm{ij,rel}}\right)=u\left(S_{\mathrm{h,rel}}\right)=k=\frac{1}{\sqrt{n}} \tag{33}$$

With $n = 5$, it results that $k = 0.45$.

According to Table 9.4 from the book

$$u(h)=\frac{\Delta h}{\sqrt{3}}$$

and applying equations 9.23 and 9.24 from the book

$$u\left(S_{\mathrm{h}}\right)=-2\,S\,\frac{u(h)}{h}. \tag{34}$$

Thus, it applies that

$$u\left(S_{\mathrm{h,rel}}\right)=\left|\frac{u\left(S_{\mathrm{h}}\right)}{u\left(S_{\mathrm{zul}}\right)}\right|$$

where according to equation 9.21 from the book:

$$u\left(S_{\mathrm{zul}}\right)=\frac{\left|\pm\Delta S_{\mathrm{zul}}\right|}{\sqrt{3}}=\frac{\left|\pm 0.1\cdot S\right|}{\sqrt{3}}=10^{-7}\,\frac{\mathrm{V}}{\mathrm{Pa}}.$$

Using equation (34), it results that

$$u\left(S_{\mathrm{h,rel}}\right)=\frac{2\,S\;\;u(h)/h}{0.1\;S/\sqrt{3}}=20\sqrt{3}\,\frac{u(h)}{h}=10\,.$$

From that, it follows that

$$u(h) = u(S_{\mathrm{h,rel}}) \cdot \frac{h}{20\sqrt{3}}$$

and using equation (33)

$$u(h) = \frac{1}{\sqrt{n}} \cdot \frac{h}{20\sqrt{3}} = \frac{0.45}{20\sqrt{3}} \cdot h = 0.13\ \mu\mathrm{m} \tag{35}$$

Using equation (35), the corresponding tolerance band will be

$$\pm \Delta h = \pm u(h) \cdot \sqrt{3} = \pm 0.23\ \mu\mathrm{m}\,.$$

Exercise 9.3

According to Exercise 9.2 from the book, a thickness deviation of $|\Delta h| \le \pm 0.1\ \mu\mathrm{m}$ is uncritical for the design. The corresponding thickness uncertainty is

$$u(h) = \frac{|\pm \Delta h|}{\sqrt{3}} = 0.058\ \mu\mathrm{m}$$

and the sensitivity impact

$$u(S_h) = -2\,S\,\frac{u(h)}{h} = 3.46 \cdot 10^{-6}\,\frac{\mathrm{V}}{\mathrm{Pa}} \cdot \frac{0.058\ \mu\mathrm{m}}{10\ \mu\mathrm{m}} = 2.01 \cdot 10^{-8}\,\frac{\mathrm{V}}{\mathrm{Pa}}\,.$$

Width tolerance *b* contributes the largest uncertainty, but even the uncertainty contribution of width *b* is completely uncritical.